Exhumation of eclogitic ophiolitic nappes in the W. Alps: New age data and implications for crustal wedge dynamics

Samuel Angiboust, Johannes Glodny

Exhumation of Eclogitic Ophiolitic Nappes in the W. Alps: New Age Data and Implications for Crustal Wedge Dynamics

Samuel Angiboust [1]
Johannes Glodny [2]

[1]*Institut de Physique du Globe de Paris, Université de Paris, F-75005 Paris, France (angiboust@ipgp.fr)*

[2]*GFZ German Research Centre for Geosciences, D-14473 Potsdam, Germany (glodnyj@gfz-potsdam.de)*

Keywords
Rb-Sr dating, Alps, Schistes Lustrés, Exhumation, Eclogite, Monviso

Abstract

The W. Alps high pressure ophiolitic terranes (Monviso and Rocciavre areas) are a natural laboratory to study processes such as nappe-stacking and crustal exhumation in the deep regions of subduction margins. We sampled each of the main shear zones, representing thrust contacts later reactivated as detachments, for petrological and Rb-Sr multi-mineral geochronological analyses. Three generations of white mica are commonly found in mylonitized metasediments with crystal cores formed during the high pressure event, a broad rim formed during decompression in the epidote blueschist facies and texturally late muscovite flakes locally lining the main foliation. Semi-brittle discrete shear zones commonly crosscut previous structures witnessing deformation at

temperatures lower than 300°C during exhumation. In spite of this apparent structural heterogeneity, homogeneous deformation ages mostly ranging between 38 and 35 Ma were obtained for all the shear zones bounding these major ophiolitic bodies. Pseudosection modeling confirms that the bulk of the shearing occurred in the epidote blueschist facies around 400-450°C and 1.0-1.5 GPa. These findings suggest that the shear zones between high pressure ophiolitic nappes were being actively mylonitized during exhumation in the lower epidote blueschist facies (25-40 km depth) between 38 and 35 Ma while some of the units forming the internal crystalline massifs (e.g. the Dora Maira Ultra High-Pressure unit) were still buried at more than 100 km depth (3-4 GPa and 34-36 Ma, according to most recent peak burial estimates). The growth of a crustal-scale duplex in the W. Alps is seen here as a consequence of basal accretion events that followed the exhumation of eclogitized coherent crustal slices in a serpentinized subduction channel. We conclude that in the study area (i) the buoyancy-driven exhumation of subducted continental crust has not been the only and decisive trigger for the exhumation of eclogitized oceanic lithosphere and (ii) continental subduction imprint on crustal wedge dynamics may have not been as instrumental as previously thought.

Introduction

The internal zones of the Western and Northwestern Alps represent a window onto deep-seated processes occurring during the closure of an oceanic basin and the entrance of a thinned continental margin (e.g. Tricart et al., 1984; Coward & Dietrich, 1989; Dal Piaz et al., 2003; Rosenbaum & Lister, 2005; Le Bayon & Ballèvre, 2006; Beltrando et al., 2010). The French-Italian part of the Alpine belt is particularly suited for studying subduction-related processes as the Oligocene collisional imprint remained

very limited, preventing full recrystallization of prograde structures and avoiding partial melting related to crustal thickening, as in the Eastern Alps (e.g. Kurz et al., 1998; O'Brien, 2001; Bousquet et al., 2008; Handy et al., 2010). Previous tectonic and geochronological studies in the French-Italian Alps extensively focused on constraining peak burial age data for the high-pressure (blueschist and eclogite-facies) nappes forming the internal metamorphic zones such as the Dora Maira ultra-high-pressure (UHP) unit (e.g. Duchêne et al., 1997) or Monviso (e.g. Rubatto & Hermann, 2003). Exhumation-related ages are more scarce in the literature (e.g. Monié & Chopin, 1991; Agard et al., 2002; Schwartz et al, 2007; Villa et al., 2014) in spite of their importance for reconstructing the last stages of the subduction of the Tethys oceanic basin under the Apulian margin as well as for understanding the tectonometamorphic evolution of the stretched continental margin when entering an active subduction margin (e.g. Polino, 1990; Guillot et al., 2009). Age data for the Alpine shear zones bounding the main thrust sheets composing the internal metamorphic zone nappes (e.g. Schistes Lustrés, Dora Maira complex; **Fig.1a**) are lacking. Such information turns out to be critical in order to refine our understanding of deep plate convergence dynamics during and after the closure of the Tethyan realm. We herein focus on the dating of the main shear zones bounding the Monviso and Rocciavre massifs, which are both exhumed remnants of the Tethyan seafloor, now stuck up between the Schistes Lustrés complex (paleo-accretionary wedge) and the Dora Maira complex (thinned European continental margin; **Fig.1a**). The significance of these ages, which challenge the common belief that the subduction of thinned continental crust critically controls the preservation of large volumes of mafic HP rocks, is herein discussed.

Geological and Structural settings

The internal metamorphic zones of the W. Alps are, in the Cottian-Piemonte regions, composed of three main domains from W to E (e.g. Schmid et al., 2004; Oberhänsli et al., 2004): the Briançonnais domain that corresponds to the stretched European margin that entered the Alpine edifice in the blueschist facies (e.g. Ambin dome), the Schistes Lustrés complex (that comprises both metasediments and meta-ophiolitic material metamorphosed at blueschist to eclogite-facies conditions; e.g. Monviso, Rocciavre) and below, the Internal Crystalline Massifs which correspond to Europe-derived continental slivers from the thinned margin that reached eclogite facies conditions during the late subduction stages. We focus here on the Schistes Lustrés (SL) complex that represents the preserved remnants of the Alpine paleo-accretionary wedge formed during the convergence between the European continent and the Apulian micro-plate from the Cretaceous until middle Eocene (Lemoine & Tricart, 1986; Deville et al., 1992 and references therein; **Fig.1a**). The associated Liguro-Piemontese realm is believed to represent a branch of the Tethys ocean (e.g. Stampfli & Marchant, 1997), now exhumed in the western Alps as composite nappes stretching from Southern Switzerland to the south-west, along the Franco-Italian border. The SL complex is characterized by a well-marked and well-documented eastwards increase of peak burial metamorphic conditions from blueschist to eclogite-facies conditions (Saliot et al., 1980; Goffé & Chopin, 1986). Blueschist-facies metamorphism prevails along the western part of the complex (e.g. Queyras region; **Fig.1a**) while eclogite-facies domains are widespread in the Piemonte area to the East (Italy), towards the bottom of the slice-stack (Lardeaux et al., 1987; Agard et al., 2001; Oberhänsli et al., 2004). This increase is commonly interpreted as reflecting the exhumation of increasingly deeper segments of

109 the alpine paleo-accretionary wedge towards the innermost regions of the SL complex
110 (e.g. Cloos & Shreve, 1988; Yamato et al., 2007).

111 High-resolution geothermo-barometric investigations have shown that the SL
112 complex is formed by discrete tectonic slivers with distinct pressure-temperature-time
113 histories (P-T-t; Fudral et al., 1987; Gabalda et al., 2009; Plunder et al., 2012; Negro et
114 al., 2013; Angiboust et al., 2014). Peak burial ages (D1 stage) estimated by Ar/Ar white
115 mica geochronology for the Western part of the SL complex cluster around 55 Ma
116 (Takeshita et al., 1994; Agard et al., 2002). The SL complex structure has been
117 interpreted as the result of superimposed subduction interface accretionary processes
118 ("underplating"; Platt, 1986) and subduction interface deformation processes (Plunder et
119 al., 2012). While it seems that along the Swiss-Italian border the original underplating
120 sequence has been tectonically re-activated possibly as a consequence of the
121 indentation with the European Briançonnais continental basement (Angiboust et al.,
122 2014), the SL complex in the Queyras region further south seems to have been mostly
123 lately tilted and domed while the thinned fragments of the Briançonnais continental
124 margin were subducted and exhumed back from eclogite-facies conditions (e.g. Henry et
125 al, 1993; Avigad et al., 1993; Ganne et al., 2006). The sequence of tectono-metamorphic
126 events in this region has been extensively studied and discussed in the literature (see
127 for example Agard et al., 2001, Tricart et al., 2004 and Ganne et al., 2006 and
128 references therein). The chronology of events can be simplified as (i) a D1 event
129 probably related to subduction, (ii) a well-developed D2 event related to exhumation and
130 (iii) a D3 event of variable intensity related to the thickening of the crustal wedge in the
131 Queyras region and to an increasingly strong collisional imprint towards Switzerland
132 (e.g. Bucher et al., 2003).

One of the striking features characterizing the eclogite-facies zones in the W and NW Alps is the presence of very long, almost coherent domains such as in the Zermatt-Saas unit, the Rocciavre or the Monviso massifs (Bucher et al., 2005; Angiboust et al., 2009, 2012a). These slivers apparently detached from the downgoing slab as tens-of-kilometers long panels in the lawsonite-eclogite facies between 50 and 45 Ma, shortly before the complete consumption of the oceanic lithosphere (Monié & Philippot, 1989; Rubatto & Hermann, 2003; Rubatto & Angiboust, 2015). In most cases, the original seafloor stratigraphy has been preserved (despite subduction down to c.80km) with from top to bottom (i) calcschists and pelitic deposits (ii) variably-thick and laterally distinct mafic intrusives and associated volcanic products (iii) a nearly fully-serpentinized lherzolitic sole ranging in thickness from several meters to a kilometer (e.g. Lombardo et al., 1978; Pognante, 1985; Angiboust & Agard, 2010; Fontana et al., 2015). In the Monviso massif in the W. Alps, two main ophiolitic sequences have been identified: the (overturned) Monviso unit and the coherent Lago Superiore Unit (Lombardo et al., 1978; Angiboust et al., 2012a; Locatelli et al., 2018). All the tectonic boundaries between these units and adjacent units (Vallanta Shear Zone: VSZ; Upper Shear Zone: USZ; Basal Shear zone: BSZ) as well as intra-Lago Superiore unit shear zones (Intermediate Shear Zone: ISZ; Lower Shear Zone: LSZ) exhibit to various degrees some dynamic metamorphic re-equilibration commonly considered as exhumation-related (**Fig.1**; **Table 1**; Schwartz et al., 2000; Angiboust et al., 2012a).

This sequence of eclogitized, ocean-derived slices is now underlain by a composite nappe-stack forming the Dora Maira s.l. massif which comprises high-pressure to ultra-high-pressure slivers separated by metasediment-bearing shear zones (e.g. Chopin et al., 1991; Michard et al., 1993; Gasco et al., 2011; Groppo et al., 2019

157 and references therein; **Fig.1b**). Peak burial P-T conditions estimated for most internal
158 crystalline massifs range from 500 to 600°C and 2 to 3 GPa (e.g. Radulescu et al., 2009;
159 Gasco et al, 2011). The youngest HP ages of the W. Alps belt (35-32 Ma), obtained for
160 the coesite-bearing Brossasco-Isasca unit (e.g. Tilton et al., 1991; Gebauer et al., 1997;
161 Duchêne et al., 1997), demonstrate that the stretched fragments of the European
162 continental margin were indeed the latest to enter and escape the deep alpine
163 subduction environment.

164 All the sequence of former thrust contacts that formed at different depths during
165 accretion along the subduction interface were commonly reactivated as normal-fault
166 detachments (e.g. Philippot, 1990; Ballèvre et al., 1990; Wheeler, 1991; Schwartz et al.,
167 2000; Le Bayon & Ballèvre, 2006; **Fig.2a**). A late recrystallization in the lower Epidote
168 Blueschist (EBS) facies at 390-450°C and 0.6-0.9 GPa has been estimated for this
169 deformation event by Schwartz et al. (2000) for the mafic rocks from the Monviso massif.
170 Similar retrograde P-T conditions (390-430°C and 0.8-1.2 GPa) were obtained for
171 retrogressed Lago Superiore unit calcschists in the Monviso massif by Angiboust et al.
172 (2012a). Agard et al. (2001) have shown using in situ Ar-Ar dating on different white
173 mica generations that the bulk of the exhumation in the SL complex nearby has been
174 achieved between blueschist and greenschist facies at 49-43 Ma (their top-to-the-east
175 phase D2). This deformation is particularly pervasive along the contacts between the
176 former thrust sheets (**Fig. 2**) where very strong mineral lineations (L-tectonites) defined
177 by blue amphibole and phengite crystals can commonly be observed (**Fig. 2b,2c**). The
178 samples selected for our geochronological work have been preferentially taken in the
179 parts of the shear zones exhibiting the strongest apparent EBS-facies overprint.

These mylonites are overprinted by semi-brittle C-S structures (**Fig.2d**) forming locally widespread, high-angle top-to-the-W shear bands along the detachments bounding the former thrust sheets (e.g. Philippot, 1990). This stage, well-marked in the Schistes Lustrés metasedimentary sequence, has been interpreted by Agard et al. (2001, 2002, their phase D3) as formed during sub-greenschist facies, brittle-plastic transition conditions (c. 300°C) between 41 and 36 Ma and corresponding to the top-to-the-W detachments earlier identified by structural investigations. The origin of this late event has been debated as some authors consider this event as thickening-related (e.g. Lagabrielle, 1987) while Ballèvre et al. (1990), Philippot (1990) and Agard et al. (2001) among others envision it as a consequence of an extensional regime associated with the late emplacement of the Dora Maira antiformal stack. Note that in our study we avoided sampling these late, low-T D3 structures as the Rb-Sr method is not suitable to directly date semi-brittle deformation.

The transition of continental subduction to collision is expected to have occurred at around 34-30 Ma as evidenced by the activation of the Penninic frontal thrust and the onset of the exhumation of internal crystalline massifs such as Dora Maira (e.g. Ford et al., 2006). The sequence of ductile events recorded in the studied area is followed by a post-30 Ma exhumation-related deformation occurring by faulting related to regional extension (Rolland et al., 2000; Schwartz et al., 2002; Agard et al., 2003; Tricart & Schwartz, 2007). Zircon fission track ages confirm that the isotherm 300°C has been crossed in the eastern Schistes Lustrés complex between 30 and 20 Ma (Schwartz et al., 2007). More recently, detrital geochronology led Mark et al. (2016) and Jourdan et al. (2013) to propose that the Dora Maira and Monviso massifs were already exposed at the surface in the time window of 30-26 Ma.

204

205 **Analytical Methods**

206 In order to quantify the chemistry of minerals forming in the selected set of
207 samples, Electron Probe Micro-Analyses (EPMA) have been performed using a Cameca
208 SX-5 at the CAMPARIS analytical facility in Paris University using standard analytical
209 conditions (15 keV, 10 nA, beam diameter between 2 and 5µm) using a set of synthetic
210 and natural crystals for calibration. X-ray maps have been acquired on the same
211 instrument using analytical conditions of 15keV, 250 nA, a counting time of 60
212 milliseconds and step size of 3µm. Fe_2O_3 (Fe), $MnTiO_3$ (Mn, Ti), diopside (Mg, Si), CaF_2
213 (F), orthoclase (Al, K), anorthite (Ca) and albite (Na) were used as standards. A
214 scanning electron microscope (SEM) Zeiss EVO MA10 at the Institut de Physique du
215 Globe de Paris using internal calibration standards was used for microscopic
216 investigations and surface composition characterization. Mineral abbreviations are after
217 Whitney & Evans (2010) except for phengite (Phg here).

218 The Rb-Sr method is reliable for dating the waning stages of dynamic
219 recrystallization of white mica in equilibrium with other, simultaneously recrystallizing Sr-
220 bearing phases (Inger and Cliff, 1994; Freeman et al. 1998), provided that no later
221 thermal-diffusive or retrogressive reactive overprint occurred. Resetting of the Rb-Sr-
222 system in white mica via diffusional processes is possible only at temperatures well
223 above 600°C (Glodny et al. 2008), whereas ductile deformation and associated
224 recrystallization may reset the Rb/Sr system of white mica at temperatures as low as
225 300°C (Müller et al. 1999). Previous studies (e.g. Bachmann et al., 2009; Angiboust et
226 al., 2014, 2016) have shown that partial re-equilibration of the Sr isotopic composition of
227 white mica may cause problems for calculating isochrons due to incomplete

mylonitization of the rock mass and inheritance of ante-mylonitization white mica porphyroclasts. One consequence of this phenomenon is the obtainment of apparently younger ages for successively smaller grain-size white mica fractions (Halama et al. 2018). Apparent ages that are calculated considering the smallest analyzed mica grain-size fractions can thus be considered as representing a maximum age estimate for the end of ductile deformation. For mineral separation work, we used small samples (less than 100 g) containing white mica as a high Rb-Sr phase. Isotopic data were generated at GFZ Potsdam on a Thermo Scientific TRITON thermal-ionization mass spectrometer. Sr isotopic composition was measured in dynamic multicollection mode. Rb isotope dilution analysis was done in static multicollection mode. The value obtained for $^{87}Sr/^{86}Sr$ in the NIST SRM 987 isotopic standard during the period of analytical work was 0.710242 ± 0.000020 (2σ, n=16). For calculation of isochron parameters, standard uncertainties of 0.005% for Sr isotopic ratios and of ± 1.5% for Rb/Sr ratios were used, provided that analytical uncertainties were smaller than these values. Else, analytical uncertainties were directly used as input parameters for calculation. Handling of mineral separates and analytical procedures are described in more detail in Glodny et al. (2008). Uncertainties of isotope and age data are quoted at 2σ throughout this work. The program ISOPLOT/EX3.71 (Ludwig, 2009) was used to calculate regression lines. The ^{87}Rb decay constant is used as recommended by Villa et al. (2015).

Micro-textural and compositional record of exhumation-related deformation

In order to understand the P-T-t conditions of retrogressive deformation, we focused our study on 6 samples from the Monviso massif and 3 samples from the Rocciavre massif, which is considered here as an analogue to the Monviso Lago

252 Superiore Unit in terms of tectonic-metamorphic history (e.g. Pognante, 1985; Philippot,
253 1990). Detailed petrographic information as well as available P-T-t information are
254 provided in **Table 1**. Thin sections were prepared in the XZ plane in order to maximize
255 the chances of identifying multiple paragenetic associations and better understand
256 structural relationships and fabric overprinting.

257 The studied Monviso massif mylonitized calcschists (and impure quartzites) have
258 been sampled in lenses in serpentinite (ISZ: Vi1807) as well as in layers (VSZ: Vi1802;
259 USZ: Vi1701; BSZ: Vi1801) within shear zones cutting through the metamorphic
260 sequence (**Table 1**). All the samples comprise chlorite-phengite-albite-quartz±calcite as
261 main retrograde, post-eclogitic minerals. White mica crystals are optically zoned. Apatite,
262 zircon, epidote, allanite, rutile or titanite, Na-Ca or Ca-amphibole and paragonite are
263 also found as part of the main foliation assemblage. Garnet is small (<200 μm),
264 unzoned, spessartine-rich ($Alm_{34}Sps_{54}Grs_{6}Prp_{6}$) and rare. Quadrangular-shaped
265 aggregates formed by chlorite and calcite crystals may be interpreted as pseudomorphs
266 after prograde chloritoid and lawsonite, respectively (for a detailed description of
267 Monviso metasediments see Angiboust et al., 2012a; see also Appendix A for further
268 petrographic information).

269 Cofacial, adjacent mafic Monviso massif lithologies (Vi1703 and Vi1704) have
270 been sampled in the Upper Shear Zone, within the metabasaltic sequence that caps the
271 continuous ophiolitic sequence described in Angiboust et al. (2012a). These two
272 samples exhibit a retrograde paragenesis mostly comprising blue amphibole,
273 clinozoisite, phengite, chlorite and albite (**Table 1**; **Fig.2**; in the EBS facies of Evans,
274 1990). In the Rocciavre massif, incipient destabilization of eclogitized meta-mafic rocks
275 led to the formation of a discrete glaucophane-omphacite-clinozoisite (possibly after

lawsonite)-phengite assemblage (Ro1601) forming shear bands cutting across the (phengite-free) eclogite-facies matrix. In the underlying “Silvery micaschists” which cap the top of the Dora Maira complex along the Rocciavre basal thrust (e.g. Sandrone et al., 1993; **Fig.1a**), a retrograde assemblage comprising phengite-chloritoid-albite-tourmaline-quartz-calcite is observed (Ro1613 and Ro1616). Sample Ro1613 was collected right on the basal Rocciavre thrust and Ro1616 was collected structurally 100m below the latter. The prograde/peak eclogite-facies garnet does not appear to be stable with the exhumation-related paragenesis in any of the studied samples. Garnet is in fact always rimmed by chlorite and replaced by chlorite or albite along cracks and rims (Appendix A).

Our microscopic investigations on all the samples selected for Rb-Sr dating led to the identification of three main phengite compositional groups, presented in **figure 3**. Representative probe analyses are given in **Table 2**. The volumetric proportion of each white mica fraction is estimated based on electron microscopy observations on the set of studied thin sections (back-scattered imaging mode; **Table 1**). Phengitic mica analyses are given here in terms of celadonite, muscovite and pyrophyllite components and shown in the diagram presented in **figure 3d**. High celadonite contents are widely accepted as a marker of high pressure-low temperature metamorphic conditions while muscovitic rims are considered as a decompression-related feature (e.g. Massonne & Schreyer, 1987). All the samples studied exhibit such common zoning pattern characterized by celadonite-richer cores (Phg1) and muscovite-richer rims (Phg2). The thickness of these rims can be variable among samples (e.g. **Fig.3a,b,c**). Phengite is systematically closely associated with chlorite flakes also parallelized along the main sample foliation. Phengite-chlorite “fishes” wrapped by the main foliation are commonly

observed (**Fig.3a**). Chlorite, which may, depending on bulk composition, have been part of the peak assemblage, also occasionally exhibits some zoning in terms of Fe/Mg ratios with darker cores and brighter, Fe-richer rims. These rims are in apparent textural equilibrium with muscovitic micas and paragonite flakes that commonly underline the main foliation (**Fig.3a**,**c**). Muscovite flakes always appear texturally late along the foliation in sheared samples and/or lining grain boundaries in exhumation-overprinted samples.

Thermobarometric constrains on phengite formation

In order to constrain the P-T conditions recorded by recrystallized phengite crystals lining the main retrogressive foliation, a pseudosection model has been calculated for the impure quartzite Vi1701 which is representative of the average micro-structural pattern record in the set of studied metasediments. A free-energy minimization approach using the software Perplex (version 6.8.1, Connolly, 2005) and the self-consistent thermodynamic database and solution models of Holland and Powell (2011 version; TC-DS61) has been chosen. Amphibole has been modeled using the Diener et al. (2007) solid solution model for clino-amphiboles. Mica was modeled using the Coggon & Holland (2002) model updated by Auzanneau et al. (2010) and garnet using the White et al. (2005) solid solution model. Feldspar was modeled following Fuhrman & Lindsley (1988), chlorite using the White et al. (2014) model and chloritoid using the model of Smye et al. (2010). We designed the model using an average of four 10mm² surface estimates acquired at the scanning electron microscope facility at IPGP. The description of this sample is given in **Table 1**. The averaged, normalized oxide weight percent composition is the following: SiO_2 (87.5), Al_2O_3 (6.5), FeO_T (1.95), MnO (0.08),

MgO (1.1), CaO (0.23), Na_2O (0.35) and K_2O (2.18). Water is considered as in excess and iron, in sake of simplicity, considered as ferrous in these calculations. Given the scarcity of carbonates in sample Vi1601, the XCO_2 fraction in the fluid phase has been set equal to zero.

This model, presented in **figure 4**, has been calculated over the P-T range 350-550°C and 0.7-2.5 GPa. Phengite isopleth distribution shows that the highest silica content region (Si > 3.5 atoms per formula unit; a.p.f.u.) is expected in the lawsonite-bearing field for upper blueschist facies conditions (above 2 GPa). Pyrope content of peak burial garnet, plotted as yellow dotted lines, is comprised between 6 and 9 mol.% for the peak metamorphic conditions of 460-500°C and 1.9 – 2.4 GPa calculated by Angiboust et al. (2012a). Such concentrations are compatible with the pyrope content analyzed in Vi1701 (c. 6 mol.%; see Appendix A for further details), thus confirming peak burial conditions near 2.3 GPa and 470°C for the Monviso unit, within the Phengite-Lawsonite-Chloritoid-(Na-)Amphibole-Garnet-Quartz field. This assemblage, almost fully overprinted in the samples selected for this study, matches with the parageneses reported and studied by Kienast (1983) and Angiboust et al. (2012a) in less overprinted samples from the same locality.

For the studied Vi1701 bulk rock composition, phengite silica contents comprised between 3.39 and 3.43 a.p.f.u. are predicted for EBS facies conditions between 1.0 and 1.7 GPa. Modeled mineral proportions for the retrogression event (given in the pie-chart on **Fig. 4**) are in relatively good agreement with modal mineral abundances observed within the impure quartzite Vi1701. The prediction of 0.5 vol.% of garnet while it is absent from the retrograde assemblage is likely an artefact due to the consideration of manganese in the bulk system. Removing Mn does not greatly impact the topology of

348 the system as well as phengite isopleth distribution. At the entrance in the greenschist
349 facies (c. 360°C and 0.7 GPa) along the P-T path considered in this study, the white
350 mica modeled for this composition has a silica content of 3.22 a.p.f.u (**Fig.4**).
351
352 **Rb-Sr geochronology: results and significance**
353 Nine samples have been selected for Rb-Sr multi-mineral analysis. The results
354 are presented in **figure 5** (for Monviso massif samples) and **figure 6** (for Rocciavre
355 region sample). The six micaschist samples from the Monviso massif are characterized
356 by a strikingly narrow deformation age range, comprised between 38.5 and 35.5 Ma,
357 considering the 2σ uncertainties on these ages. All these samples (except Vi1802)
358 overlap in age around 37 Ma (see the full dataset in Appendix B). Isochron plots indicate
359 that in some samples there is a minor correlation between white mica grain size and the
360 isotopic age signature of individual mica fractions. When present (e.g. Vi1701, Vi1801,
361 Vi1807), this correlation may reflect multiple white mica recrystallization events as a
362 consequence of partial tectonic re-activation after the main D2 deformation event
363 recorded in the sample (**Figs 5 and 7**; see Appendix B for further details and
364 calculations of various two-points isochrons using different grain size fractions). In other
365 samples such correlations are insignificant or absent (e.g. Vi1704a, Vi1802). Given the
366 mylonitic texture of these rocks, we interpret these age data as deformation ages,
367 related to the main exhumation-related shearing event (the D2 event from Agard et al.,
368 2001).
369 The youngest Monviso region age of 35.75 +/- 0.56 Ma has been sampled on the
370 Vallanta Shear zone (VSZ on **Fig.1b**) on an outcrop crosscut by numerous top-to-the-W
371 extensional shear zones (**Fig.2d**). The highest proportion of muscovitic micas (>95

372 vol.%) has been observed for this sample (Vi1802; **Fig.7**). We hypothesize that this
373 slightly younger age is the result of a more penetrative re-equilibration associated with
374 the activity of this detachment which clearly postdates all previous exhumation-related
375 structures. A similarly young, late re-equilibration signal has been also detected in
376 Vi1701, Vi1801 and Vi1807 using the smallest mica fractions, yielding 2 points-isochron
377 ages ranging between 34 and 35.5 Ma (see Appendix B for calculation details). Note that
378 the late, narrow shear bands as shown in **figure 2d** were not investigated using Rb-Sr
379 dating as the textures clearly point to a LT (<300°C) deformation regime implying
380 possibly micro-structural inheritance, and potential lack of readjustment of the Rb-Sr age
381 system.

382 Only one sample from the core of the Rocciavre eclogitic metagabbro body yields
383 an age of 46.3 ± 2.8 Ma significantly older than other ages obtained. This event is
384 represented in the sample by a high-pressure assemblage comprising omphacite
385 intergrown with phengite and blue amphibole (**Table 1**). The stability of omphacite,
386 instead of plagioclase or hornblende as expected for alpine retrogressed assemblages,
387 shows that this sample recrystallized at high pressure (1.5 to 2.5 GPa), thus possibly
388 marking the incipient decompression stage shortly after detachment from the downgoing
389 oceanic slab. The age of the Rocciavre metagabbro peak burial could not be evaluated
390 due to the absence of phengite in unretrogressed garnet-omphacite-rutile lithologies. We
391 however postulate that a peak burial age in the range 50-45 Ma, similar to the Monviso
392 Lago Superiore unit, is very likely from the extreme similarity in structural and
393 mineralogical evolution (e.g. Pognante, 1985). If correct, this postulate would confirm
394 that our 49.1-43.5 Ma age range (considering the 2σ uncertainty) indeed corresponds to

395 an early re-equilibration stage shortly after peak conditions as suggested by the rock
396 micro-structures.

397 The last two samples have been collected near the contact between the meta-
398 ophiolitic Rocciavre nappe and the underlying “Silvery micaschist” unit, which
399 corresponds to a slice of HP felsic and metasedimentary material interpreted as part of
400 the cover of the Dora Maira (poly-)metamorphic basement (e.g. Pognante & Sandrone,
401 1989). Sample Ro16-13, which comes from the shear zone itself, exhibits an age of 35.4
402 ± 2.3 Ma, substantially younger than the age estimated for sample Ro16-16 (39.5 ± 0.4
403 Ma) collected hundred meters below Ro16-13, towards the core of the Silvery micaschist
404 unit. This age difference is supported by the higher silica content of phengite crystals
405 from sample Ro16-16 foliation (**Fig.6**), which has likely been less affected than Ro16-13
406 by late exhumation-related re-equilibration.

407 From this new age dataset, the most striking feature is the prevalence of 38-36
408 Ma ages among the four shear zones sampled. The ages presented here are interpreted
409 as reflecting the waning stages of ductile deformation. The bulk of the dynamic
410 recrystallization along the shear zones bounding the HP ophiolitic nappes in the internal
411 W. Alps apparently stopped at 36-35 Ma, when the rocks were at the transition between
412 epidote blueschist and greenschist-facies at c.400°C (see the P-T-t path in **Figs 4 and**
413 **7**). Some later, localized extension of minor kinematic importance occurred with
414 relatively minor effect on the main exhumation stage recorded in the studied samples
415 here. When such late imprint is present, slightly younger ages near 35 Ma (e.g. Vi1801,
416 Vi1807, Ro1613) are obtained due to re-equilibration of the HP phengite to muscovite
417 (Si < 3.15 a.p.f.u.; **Figs 3 and 7;** Appendix B; see also Freeman et al., 1997). Such low
418 celadonite content white micas are expected to crystallize for a metapelitic system at

pressures much below 1 GPa (see for example the pseudosection for the Monviso metapelite C32 in Angiboust et al., 2012a; their figure 8). We interpret the relatively young ages calculated for these samples as the record of the latest ductile, greenschist facies deformation increment (measurable with the Rb-Sr method) before the crossing of the brittle-ductile transition at c.350°C (**Fig.7**).

Last, we note that the age range for the main retrogressive deformation recorded by Monviso/Rocciavre shear zones is substantially younger (c.10 Ma) than the D2 deformation event previously dated using in situ Ar-Ar laser ablation on phengite crystals from the SL paleo-accretionary complex in the Queyras region (51-45 Ma; Agard et al., 2002). This difference may either arise from the fact that the structures preserved in the western part of the SL paleo-accretionary complex could be older than those from the innermost SL complex in the Monviso region. A minor contribution from inherited Ar in their results cannot be excluded as well.

Emplacement model and tectonic implications

A tentative model on the exhumation dynamics along HP shear zones in the studied region of the W. Alps, gathering age data from the literature together with our new results, is presented in **figure 8**. After detachment from the downgoing slab at c.45 Ma in the eclogite facies (P>2.5 GPa), the Rocciavre and Lago Superiore units were likely coherently exhumed along the plate interface via subduction channel dynamics (e.g. Guillot et al., 2009) assisted by the buoyant serpentinite sole attached to them (e.g. Hermann et al., 2000; Schwartz et al., 2001; Angiboust et al., 2012b; Ruh et al., 2015; Gilio et al., 2019). Even though the duration of this part of the exhumation path is not precisely constrained, one can postulate that it lasted up to 7 Ma (i.e. the time span

443 between the peak burial imprint at 45 Ma and the oldest of our retrogressive ages at
444 around 38 Ma; Rubatto & Angiboust, 2015; this work; see **Fig.8**). Such long residence
445 time possibly contributed to the pervasive eclogite-facies recrystallization stage well
446 visible in rocks from the Lago Superiore unit.

447 The overturned Monviso unit sequence (with the sedimentary cover at the base
448 and the ultramafic sole forming the top of the Monviso mountain; Lombardo et al., 1978)
449 detached from the downgoing plate at c.2.3 GPa. Unfortunately, the peak burial age is
450 still lacking. The very subtle eclogite-facies imprint recorded in the Monviso unit
451 sequence makes difficult any geochronological approach despite peak burial
452 temperatures near 480°C (Angiboust et al., 2012a). One possibility to explain the
453 scarcity of eclogite-facies index minerals can be a relatively short residence time in the
454 high-pressure domain (together with a less pervasive eclogitic deformation imprint; e.g.
455 Lombardo et al., 1978). The tectonic juxtaposition between the Monviso and Lago
456 Superiore units occurred between 1.5 and 2 GPa (Angiboust et al., 2011; **Fig.8**). Our
457 multi-mineral Rb-Sr isochron patterns record only very minor isotopic inheritance effects
458 from prograde-to-peak high-Si cores on the isochron (e.g. **Figs.5 and 6**). This statement
459 confirms that the near-peak burial conditions (where the highest-Si phengite crystallized;
460 e.g. **Fig.3b**) were reached only shortly before the EBS imprint shearing responsible for
461 the bulk of the retrogression of the matrix (stage D2 from Agard et al., 2001 and Tricart &
462 Schwartz, 2006; **Figs.2c, 3b**). In the absence of peak burial age data for the Monviso
463 unit, we thus speculate that (i) the Monviso unit detached from the downgoing Tethyan
464 slab shortly before the obtained exhumation age, possibly near c.40 Ma and that (ii) the
465 EBS overprint occurred only a few millions years after the detachment of the Monviso
466 unit from the downgoing slab (**Fig.8**). Further studies should aim at constraining peak

burial metamorphic ages for Monviso (*sensu stricto*) and Rocciavre units using other geochronological techniques in order to better quantify exhumation velocities and P-T-t trajectories for these two units.

One of the main findings of this work is that ductile deformation in all the shear zones separating the main thrust sheets (i.e. the D2 stage) coevally came to stop at around 36-35 Ma. The prevalent D2 imprint recorded by these shear zones in the time range 38-36 Ma was the consequence of kinematic inversion enabling the unroofing of the deep-seated regions of the Alpine paleo-accretionary wedge (**Fig.8**; e.g. Philippot et al., 1990; see also Reddy et al., 1999; Ring & Glodny, 2010). Another fundamental implication is that this 38-36 Ma age range is older than the 36-33 Ma time window commonly reported for the peak burial conditions of the Internal crystalline massifs such as in the Dora Maira UHP unit (Gebauer et al., 1997; Duchêne et al., 1997; Rubatto & Hermann, 2001; Di Vicenzo et al., 2006). This information reveals that relatively shallow conditions (i.e. lower EBS facies; c.25 km depth; **Fig.8**) were already reached by the rocks forming the paleo-accretionary antiformal stack *before* the attainment of peak burial conditions (depth >70km) by the thinned European continental margin of the Briançonnais domain (i.e. the Internal crystalline massifs). Recent P-T-time paths for some of the other tectonic elements forming the Dora Maira complex (e.g. Pinerolo-Sanfront or Dronero-Sampeyre units; **Fig.1a**) are lacking. If some of these nappes have undergone metamorphism earlier than the Dora Maira UHP unit (**Fig.1a**), they would have certainly impacted the deep emplacement dynamics (e.g. Groppo et al., 2019 and references therein) with consequences on the exhumation of the large eclogite-facies slivers such as Monviso or Rocciavre massifs. Note that the current absence of agreement among published peak burial ages for the Gran Paradiso massif (e.g. 43 ±

491 0.5 Ma: Meffan-Main et al., 2004: 33.7 ± 1.6 Ma, Radulescu et al., 2009; 41-34 Ma:
492 Rosenbaum et al., 2012) does not enable generalizing this statement to the entire W.
493 Alps internal zones as far as Aosta valley region 150 km northwards.

494 It is therefore envisioned that the exhumation of the HP-UHP rocks from the
495 former stretched European margin is not responsible, at least in the study area, for the
496 deep exhumation of the eclogite-facies ophiolitic terranes (as proposed by Lapen et al.,
497 2007 for the continental Monte Rosa and ophiolitic Zermatt-Saas units in the NW Alps,
498 for instance). Our results, in line with Duchêne et al. (1997) and compatible with the data
499 from Gasco et al. (2011, 2013), suggest instead that the exhumation of the internal
500 crystalline massifs such as the Dora Maira UHP unit have at most contributed to the
501 partial re-activation of former thrust contacts as detachments in the greenschist facies
502 and above (**Fig.8**). In other words, the crustal-scale antiformal structure shaping the W.
503 Alps internal zones is therefore not the sole consequence of the exhumation of deeply
504 subducted continental units. The accretionary edifice may already have acquired a large
505 part of its antiformal structure during early Cenozoic times through a long-lasting basal
506 accretion sequence (e.g. Platt, 1986; Angiboust et al., 2014). Future geochronological
507 investigations should clarify the tectonic relationships between Monte Rosa, Gran
508 Paradiso and Zermatt-Saas units further north and evaluate whether our model also
509 applies for this setting in the NW Alps.

510 Similar dynamics are widely reported in other, including present-day subduction
511 margins such as along the circum-Pacific domain (e.g. Platt, 1986; Kimura et al., 1996;
512 Glodny et al., 2005; Willner, 2005; Menant et al., 2019; see also Agard et al., 2018 and
513 references therein). Note that the juxtaposition of tectonic slivers with very distinct P-T
514 paths in the basal accretion region requires complex basal “tectonic insertion”

515 mechanisms in order to explain the increasing metamorphic grade in the Schistes
516 Lustrés from W to E (e.g. Plunder et al., 2012). Such process, which is neither well
517 understood nor numerically modeled so far, requires the physical connection of the
518 updip end of the subduction channel together with the basal accretion site to enable the
519 incorporation of very high grade metamorphic elements in a lower grade slice-stack.
520 Last, the plastic recrystallization along the main structures forming this large
521 duplex ended shortly after the entrance in the greenschist facies at the latest at 35 Ma
522 while the rocks forming the stack were crossing the brittle-ductile transition (**Fig.8**). The
523 late top-to-the-W shearing visible on the roof of Monviso unit and Dora Maira complex
524 (Ballèvre et al., 1990; Wheeler, 1991; Philippot, 1990; Agard et al., 2002; **Fig.2d**) may
525 have continued to accommodate further localized extensional deformation later on near
526 the brittle-ductile transition likely as a consequence of the fast exhumation of the
527 youngest elements forming the Dora Maira complex. Zircon fission track and titanite U-
528 Pb dating confirm that the eastern part of the Schistes Lustrés and the Dora Maira
529 complex shared a common tectonic history after c.31 Ma on their way from greenschist
530 facies below c.300°C towards the surface (**Fig.8**; Gebauer et al., 1997; Rubatto &
531 Hermann, 2001; Schwartz et al., 2007).
532
533 **Conclusions**
534 The Rb-Sr multi-mineral isochron ages have been calculated for the main shear
535 zones bounding the eclogite-facies nappes in the Monviso and Rocciavre massifs (W.
536 Alps). The white micas from the metasediments in these shear zones record in a narrow
537 time frame the re-equilibration history from eclogite-facies conditions down to
538 greenschist facies through a dominant epidote-blueschist facies imprint. We show here

539 with an unprecedented resolution that this epidote-blueschist facies shearing event
540 occurred contemporaneously along all these contacts at 1-1.5 GPa, 400-450°C and in a
541 narrow age range of 38-36 Ma. Further localized deformation likely continued up to the
542 brittle-plastic transition until c.35 Ma. The high-pressure ophiolitic nappe-stack was
543 already undergoing exhumation at c.30 km depth while the deepest elements of the
544 Dora Maira massif were being subducted down to UHP conditions. We conclude that, at
545 least in the studied area, (i) basal accretion and subduction channel dynamics played a
546 key role during the early tectonic evolution of HP ophiolitic nappes (ii) the exhumation of
547 internal crystalline massifs such as the Dora Maira UHP unit impacted only lately –
548 possibly in the 33-30 Ma time window - the previously formed crustal-scale antiformal-
549 stack through the shuffling of previous thrust contacts, doming as well as via detachment
550 faulting. Our results pave the way for better understanding deep accretionary processes,
551 in particular in the context of the subduction of a stretched continental margin (e.g.
552 Crete, Sunda, Taïwan, Oman).
553
554
555 **Acknowledgements**
556 A. Cambeses, A. Plunder and J. Muñoz are acknowledged for assistance at various
557 steps of this project. This is IPGP contribution #40xx. This work has been funded by an
558 IDEX research chair to S.A. The two reviewers B. Le Bayon and P. Starr as well as the
559 special issue editor P. Agard are acknowledged for insightful comments on the
560 manuscript.
561
562 **References**

563 Agard, P., Jolivet, L., & Goffe, B. (2001). Tectonometamorphic evolution of the Schistes Lustres
564 Complex; implications for the exhumation of HP and UHP rocks in the Western Alps. *Bulletin*
565 *de la Société géologique de France*, *172*(5), 617-636.
566
567 Agard, P., Monié, P., Jolivet, L., & Goffé, B. (2002). Exhumation of the Schistes Lustrés complex: in
568 situ laser probe 40Ar/39Ar constraints and implications for the Western Alps. *Journal of*
569 *metamorphic Geology*, *20*(6), 599-618.
570
571 Agard, P., Fournier, M., & Lacombe, O. (2003). Post-nappe brittle extension in the inner Western Alps
572 (Schistes Lustrés) following late ductile exhumation: a record of synextension block rotation?
573 *Terra Nova*, *15*(5), 306-314.
574
575 Agard, P., Plunder, A., Angiboust, S., Bonnet, G., & Ruh, J. (2018). The subduction plate interface:
576 rock record and mechanical coupling (from long to short timescales). *Lithos*, *320*, 537-566.
577
578 Angiboust, S., Agard, P., Jolivet, L., & Beyssac, O. (2009). The Zermatt-Saas ophiolite: the largest
579 (60-km wide) and deepest (c. 70–80 km) continuous slice of oceanic lithosphere detached from
580 a subduction zone?. T*erra Nova*, *21*(3), 171-180.
581
582 Angiboust, S., & Agard, P. (2010). Initial water budget: the key to detaching large volumes of
583 eclogitized oceanic crust along the subduction channel?. *Lithos*, *120*(3-4), 453-474.
584
585 Angiboust, S., Agard, P., Raimbourg, H., Yamato, P., & Huet, B. (2011). Subduction interface
586 processes recorded by eclogite-facies shear zones (Monviso, W. Alps). *Lithos*, *127*(1-2), 222-
587 238.
588

589 Angiboust, S. (2011) Couplages profonds et comportement de la lithosphere océanique dans les
590 zones de subduction: approche pétrologique et thermomécanique, *PhD Thesis*, UPMC, 310p.
591
592 Angiboust, S., Langdon, R., Agard, P., Waters, D., & Chopin, C. (2012a). Eclogitization of the
593 Monviso ophiolite (W. Alps) and implications on subduction dynamics. *Journal of Metamorphic*
594 *Geology*, *30*(1), 37-61.
595
596 Angiboust, S., Wolf, S., Burov, E., Agard, P., & Yamato, P. (2012b). Effect of fluid circulation on
597 subduction interface tectonic processes: Insights from thermo-mechanical numerical modelling.
598 *Earth and Planetary Science Letters*, *357*, 238-248.
599
600 Angiboust, S., Glodny, J., Oncken, O., & Chopin, C. (2014). In search of transient subduction
601 interfaces in the Dent Blanche–Sesia Tectonic System (W. Alps). *Lithos*, *205*, 298-321.
602
603 Angiboust, S., Agard, P., Glodny, J., Omrani, J., & Oncken, O. (2016). Zagros blueschists: Episodic
604 underplating and long-lived cooling of a subduction zone. *Earth and Planetary Science Letters*,
605 *443*, 48-58.
606
607 Avigad, D., Chopin, C., Goffe, B., & Michard, A. (1993). Tectonic model for the evolution of the
608 western Alps. *Geology*, *21*(7), 659-662.
609
610 Bachmann, R., Glodny, J., Oncken, O., & Seifert, W. (2009). Abandonment of the South Penninic–
611 Austroalpine palaeosubduction zone, Central Alps, and shift from subduction erosion to
612 accretion: constraints from Rb/Sr geochronology. *Journal of the Geological Society*, *166*(2),
613 217-231.
614

615 Ballèvre, M., Lagabrielle, Y., & Merle, O. (1990). Tertiary ductile normal faulting as a consequence of
616 lithospheric stacking in the western Alps. *Mémoires de la Société géologique de France*, *156*,
617 227-236.
618
619 Beltrando, M., Lister, G. S., Rosenbaum, G., Richards, S., & Forster, M. A. (2010). Recognizing
620 episodic lithospheric thinning along a convergent plate margin: The example of the Early
621 Oligocene Alps. *Earth-Science Reviews*, *103*(3-4), 81-98.
622
623 Bousquet, R., Oberhänsli, R., Goffé, B., Wiederkehr, M., Koller, F., Schmid, S. M., ... & Martinotti, G.
624 (2008). Metamorphism of metasediments at the scale of an orogen: a key to the Tertiary
625 geodynamic evolution of the Alps. *Geological Society, London, Special Publications*, *298*(1),
626 393-411.
627
628 Bucher, K., Fazis, Y., De Capitani, C., & Grapes, R. (2005). Blueschists, eclogites, and
629 decompression assemblages of the Zermatt-Saas ophiolite: High-pressure metamorphism of
630 subducted Tethys lithosphere. *American mineralogist*, *90*(5-6), 821-835.
631
632 Bucher, S., Schmid, S. M., Bousquet, R., & Fügenschuh, B. (2003). Late-stage deformation in a
633 collisional orogen (Western Alps): nappe refolding, back-thrusting or normal faulting?. *Terra*
634 *Nova*, *15*(2), 109-117.
635
636 Chopin, C., Henry, C., & Michard, A. (1991). Geology and petrology of the coesite-bearing terrain,
637 Dora Maira massif, Western Alps. *European Journal of Mineralogy*, *3*(2), 263-291.
638
639 Cloos, M., & Shreve, R. L. (1988). Subduction-channel model of prism accretion, melange formation,
640 sediment subduction, and subduction erosion at convergent plate margins: 1. Background and
641 description. *Pure and Applied Geophysics*, 128(3-4), 455-500.

642

643 Coggon, R., & Holland, T. J. B. (2002). Mixing properties of phengitic micas and revised
644 garnet-phengite thermobarometers. *Journal of Metamorphic Geology*, *20*(7), 683-696.
645
646 Connolly, J. A. (2005). Computation of phase equilibria by linear programming: a tool for geodynamic
647 modeling and its application to subduction zone decarbonation. *Earth and Planetary Science*
648 *Letters*, *236*(1-2), 524-541.
649
650 Coward, M., & Dietrich, D. (1989). Alpine tectonics—an overview. *Geological Society, London,*
651 *Special Publications*, *45*(1), 1-29.
652
653 Dal Piaz, G. V., Bistacchi, A., & Massironi, M. (2003). Geological outline of the Alps. *Episodes*, *26*(3),
654 175-180.
655
656 Deville, E., Fudral, S., Lagabrielle, Y., Marthaler, M., & Sartori, M. (1992). From oceanic closure to
657 continental collision: A synthesis of the" Schistes lustrés" metamorphic complex of the Western
658 Alps. *Geological Society of America Bulletin*, *104*(2), 127-139.
659
660 Di Vincenzo, G., Tonarini, S., Lombardo, B., Castelli, D., & Ottolini, L. (2006). Comparison of 40Ar–
661 39Ar and Rb–Sr data on phengites from the UHP Brossasco–Isasca Unit (Dora Maira Massif,
662 Italy): implications for dating white mica. *Journal of Petrology*, *47*(7), 1439-1465.
663
664 Diener, J. F. A., Powell, R., White, R. W., & Holland, T. J. B. (2007). A new thermodynamic model for
665 clino-and orthoamphiboles in the system Na2O–CaO–FeO–MgO–Al2O3–SiO2–H2O–O.
666 *Journal of Metamorphic Geology*, 25(6), 631-656.
667
668

669 Duchêne, S., Blichert-Toft, J., Luais, B., Télouk, P., Lardeaux, J. M., & Albarede, F. (1997). The Lu–Hf
670 dating of garnets and the ages of the Alpine high-pressure metamorphism. *Nature*, *387*(6633),
671 586.
672
673 Evans, B. W. (1990). Phase relations of epidote-blueschists. *Lithos*, *25*(1-3), 3-23.
674
675 Fontana, E., Tartarotti, P., Panseri, M., & Buscemi, S. (2015). Geological map of the Mount Avic
676 massif (western Alps Ophiolites). *Journal of Maps*, 11(1), 126-135.
677
678 Ford, M., Duchêne, S., Gasquet, D., & Vanderhaeghe, O. (2006). Two-phase orogenic convergence
679 in the external and internal SW Alps. *Journal of the Geological Society*, *163*(5), 815-826.
680
681 Freeman, S. R., Butler, R. W. H., Cliff, R. A., Inger, S., & Barnicoat, A. C. (1998). Deformation
682 migration in an orogen-scale shear zone array: an example from the basal Briançonnais thrust,
683 internal Franco-Italian Alps. *Geological Magazine*, *135*(3), 349-367.
684
685 Freeman, S. R., Inger, S., Butler, R. W. H., & Cliff, R. A. (1997). Dating deformation using Rb-Sr in
686 white mica: Greenschist facies deformation ages from the Entrelor shear zone, Italian Alps.
687 *Tectonics*, 16(1), 57-76.
688
689 Fudral, S., Deville, E. & Marthaler, M., 1987. Distinction de trois ensembles d'unités dans les
690 "Schistes lustrés" compris entre la Vanoise et le Val de Suse (Alpes franco-italiennes
691 septentrionales): aspects lithostratigraphiques, paléogéographiques et géodynamiques.
692 Comptes Rendus de l'Académie des Sciences de Paris, 305, 467–472.
693
694 Fuhrman, M.L., Lindsley, D.H., 1988. Ternary-feldspar modeling and thermometry. *American*
695 *Mineralogist* 73(3-4), 201-215.

696

697 Gabalda, S., Beyssac, O., Jolivet, L., Agard, P., & Chopin, C. (2009). Thermal structure of a fossil
698 subduction wedge in the Western Alps. *Terra Nova*, *21*(1), 28-34.
699
700 Ganne, J., Marquer, D., Rosenbaum, G., Bertrand, J. M., & Fudral, S. (2006). Partitioning of
701 deformation within a subduction channel during exhumation of high-pressure rocks: a case
702 study from the Western Alps. *Journal of Structural Geology*, *28*(7), 1193-1207.
703
704 Gasco, I., Gattiglio, M., & Borghi, A. (2013). Review of metamorphic and kinematic data from Internal
705 Crystalline Massifs (Western Alps): PTt paths and exhumation history. *Journal of*
706 *Geodynamics*, *63*, 1-19.
707
708 Gasco, I., Gattiglio, M., & Borghi, A. (2011). Lithostratigraphic setting and PT metamorphic evolution
709 for the Dora Maira Massif along the Piedmont Zone boundary (middle Susa Valley, NW Alps).
710 *International Journal of Earth Sciences*, *100*(5), 1065-1085.
711
712 Gebauer, D. H. P. S., Schertl, H. P., Brix, M., & Schreyer, W. (1997). 35 Ma old ultrahigh-pressure
713 metamorphism and evidence for very rapid exhumation in the Dora Maira Massif, Western
714 Alps. *Lithos*, *41*(1-3), 5-24.
715
716 Gilio, M., Scambelluri, M., Agostini, S., Godard, M., Pettke, T., Agard, P., Locatelli, M. & Angiboust, S.
717 (2019). Fingerprinting and relocating tectonic slices along the plate interface: Evidence from
718 the Lago Superiore unit at Monviso (Western Alps). *Lithos*, 105308.
719
720 Glodny, J., Kühn, A., & Austrheim, H. (2008). Diffusion versus recrystallization processes in Rb–Sr
721 geochronology: isotopic relics in eclogite facies rocks, Western Gneiss Region, Norway.
722 *Geochimica et Cosmochimica Acta*, *72*(2), 506-525.

723

724 Glodny, J., Lohrmann, J., Echtler, H., Gräfe, K., Seifert, W., Collao, S., & Figueroa, O. (2005). Internal
725 dynamics of a paleoaccretionary wedge: insights from combined isotope tectonochronology
726 and sandbox modelling of the South-Central Chilean forearc. *Earth and Planetary Science*
727 *Letters*, *231*(1-2), 23-39.

728

729 Goffe, B., & Chopin, C. (1986). High-pressure metamorphism in the Western Alps: zoneography of
730 metapelites, chronology and consequences. *Schweizerische mineralogische und*
731 *petrographische Mitteilungen*, *66*(1-2), 41-52.

732

733 Groppo, C., Ferrando, S., Gilio, M., Botta, S., Nosenzo, F., Balestro, G., ... & Rolfo, F. (2019) What's
734 in the sandwich? New P–T constraints for the (U) HP nappe stack of southern Dora-Maira
735 Massif (Western Alps). *European Journal of Mineralogy*. In press.

736

737 Groppo, C., & Castelli, D. (2010). Prograde P–T evolution of a lawsonite eclogite from the Monviso
738 meta-ophiolite (Western Alps): dehydration and redox reactions during subduction of oceanic
739 FeTi-oxide gabbro. *Journal of Petrology*, *51*(12), 2489-2514.

740

741 Guillot, S., Hattori, K., Agard, P., Schwartz, S., & Vidal, O. (2009). Exhumation processes in oceanic
742 and continental subduction contexts: a review. In *Subduction zone geodynamics* (pp. 175-205).
743 Springer, Berlin, Heidelberg.

744

745 Guillot, S., Schwartz, S., Hattori, K., Auzende, A., & Lardeaux, J. (2004). The Monviso ophiolitic
746 massif (Western Alps), a section through a serpentinite subduction channel. *Journal of the*
747 *Virtual Explorer*, *16*, 17-pages.

748

749 Halama, R., Glodny, J., Konrad-Schmolke, M., Sudo, M. (2018): Rb-Sr and in situ 40 Ar/ 39 Ar dating
750 of exhumation-related shearing and fluid-induced recrystallization in the Sesia zone (Western
751 Alps, Italy). - *Geosphere*, 14, 4, p. 1425-1450.
752
753 Handy, M. R., Schmid, S. M., Bousquet, R., Kissling, E., & Bernoulli, D. (2010). Reconciling plate-
754 tectonic reconstructions of Alpine Tethys with the geological–geophysical record of spreading
755 and subduction in the Alps. *Earth-Science Reviews*, *102*(3-4), 121-158
756
757 Henry, C., Michard, A., & Chopin, C. (1993). Geometry and structural evolution of ultra-high-pressure
758 and high-pressure rocks from the Dora-Maira massif, Western Alps, Italy. *Journal of Structural*
759 *Geology*, *15*(8), 965-981.
760
761 Hermann, J., Müntener, O., & Scambelluri, M. (2000). The importance of serpentinite mylonites for
762 subduction and exhumation of oceanic crust. *Tectonophysics*, *327*(3-4), 225-238.
763
764 Holland, T. J. B., & Powell, R. T. J. B. (1998). An internally consistent thermodynamic data set for
765 phases of petrological interest. *Journal of metamorphic Geology*, *16*(3), 309-343.
766
767 Inger, S., & Cliff, R. A. (1994). Timing of metamorphism in the Tauern Window, Eastern Alps: Rb-Sr
768 ages and fabric formation. *Journal of metamorphic Geology*, *12*(5), 695-707.
769
770 Jourdan, S., Bernet, M., Tricart, P., Hardwick, E., Paquette, J. L., Guillot, S., ... & Schwartz, S. (2013).
771 Short-lived, fast erosional exhumation of the internal western Alps during the late early
772 Oligocene: Constraints from geothermochronology of pro-and retro-side foreland basin
773 sediments. *Lithosphere*, *5*(2), 211-225.
774

775 Kienast, J., 1983. Le métamorphisme de haute pression et basse température (éclogites et schistes
776 bleus) : données nouvelles sur la pétrologie des roches de la croute océanique subductée et
777 des sédiments associés. PhD Université Pierre et Marie Curie, Paris.
778
779 Kimura, G., Maruyama, S., Isozaki, Y., & Terabayashi, M. (1996). Well-preserved underplating
780 structure of the jadeitized Franciscan complex, Pacheco Pass, California. *Geology*, 24(1), 75-
781 78.
782
783 Kurz, W., Neubauer, F., & Dachs, E. (1998). Eclogite meso-and microfabrics: implications for the
784 burial and exhumation history of eclogites in the Tauern Window (Eastern Alps) from PTd
785 paths. *Tectonophysics*, *285*(1-2), 183-209.
786
787 Lagabrielle, Y. (1987) – Les ophiolites: marqueurs de l'histoire tectonique des domaines océaniques.
788 PhD thesis, Brest University.
789
790 Lapen, T. J., Johnson, C. M., Baumgartner, L. P., Dal Piaz, G. V., Skora, S., & Beard, B. L. (2007).
791 Coupling of oceanic and continental crust during Eocene eclogite-facies metamorphism:
792 evidence from the Monte Rosa nappe, western Alps. *Contributions to Mineralogy and*
793 *Petrology*, *153*(2), 139-157.
794
795 Lardeaux, J. M., Nisio, P., & Boudeulle, M. (1987). Deformational and metamorphic history at the
796 Lago Superiore area of the Monviso ophiolitic complex (Italian Western Alps): a record of
797 subduction–collision cycle. *Ofioliti*, *12*(3), 479-502.
798
799 Le Bayon, B., & Ballevre, M. (2006). Deformation history of a subducted continental crust (Gran
800 Paradiso, Western Alps): continuing crustal shortening during exhumation. *Journal of Structural*
801 *Geology*, *28*(5), 793-815.

Lemoine, M., & Tricart, P. (1986). Les Schistes lustrés piémontais des Alpes occidentales: approche stratigraphique, structurale et sédimentologique. *Eclogae Geologicae Helvetiae*, 79(2), 271-294.

Locatelli, M., Verlaguet, A., Agard, P., Federico, L., & Angiboust, S. (2018). Intermediate-depth brecciation along the subduction plate interface (Monviso eclogite, W. Alps). *Lithos*, *320*, 378-402.

Lombardo, B., Nervo, R., Compagnoni, R., Messiga, B., Kienast, J. R., Mevel, C., ... & Lanza, R. (1978). Osservazioni preliminari sulle ofioliti metamorfiche del Monviso (Alpi Occidentali). *Rend. Soc. Ital. Mineral. Petrol*, *34*(2), 253-305.

Ludwig, K. R. (2003). User's manual for isoplot 3.00, a geochronlogical toolkit for microsoft excel. *Berkeley Geochronl. Cent. Spec. Publ.*, *4*, 25-32.

Mark, C., Cogné, N., & Chew, D. (2016). Tracking exhumation and drainage divide migration of the Western Alps: A test of the apatite U-Pb thermochronometer as a detrital provenance tool. *Bulletin*, *128*(9-10), 1439-1460.

Massonne, H. J., & Schreyer, W. (1987). Phengite geobarometry based on the limiting assemblage with K-feldspar, phlogopite, and quartz. *Contributions to Mineralogy and Petrology*, *96*(2), 212-224.

Meffan-Main, S., Cliff, R. A., Barnicoat, A. C., Lombardo, B., & Compagnoni, R. (2004). A Tertiary age for Alpine high-pressure metamorphism in the Gran Paradiso massif, Western Alps: A Rb–Sr microsampling study. *Journal of Metamorphic Geology*, *22*(4), 267-281.

Menant, A., Angiboust, S., & Gerya, T. (2019). Stress-driven fluid flow controls long-term megathrust strength and deep accretionary dynamics. *Scientific reports*, *9*(1), 9714.

Monié, P., & Philippot, P. (1989). $^{39}Ar/^{40}Ar$ dating in the Dora Maira and Monviso massifs (Western Alps): evidence for two stages of eclogitic metamorphism. In *Terra Abstracts* (Vol. 1, p. 264).

Monie, P., & Chopin, C. (1991). $^{40}Ar/^{39}Ar$ dating in coesite-bearing and associated units of the Dora Maira massif, Western Alps. *European Journal of Mineralogy*, 239-262.

Müller, W., Dallmeyer, R.D., Neubauer, F., & Thöni, M. (1999) Deformation-induced resetting of Rb/Sr and 40Ar/39Ar mineral systems in a low-grade, polymetamorphic terrane (Eastern Alps, Austria): *Journal of the Geological Society*, 156, 261–278.

Negro, F., Bousquet, R., Vils, F., Pellet, C. M., & Hänggi-Schaub, J. (2013). Thermal structure and metamorphic evolution of the Piemont-Ligurian metasediments in the northern Western Alps. *Swiss Journal of Geosciences*, *106*(1), 63-78.

Tricart, P., & Lemoine, M. (1986). From faulted blocks to megamullions and megaboudins: Tethyan heritage in the structure of the Western Alps. *Tectonics*, *5*(1), 95-118.

O'Brien, P. J. (2001). Subduction followed by collision: Alpine and Himalayan examples. *Physics of the Earth and Planetary Interiors*, *127*(1-4), 277-291.

Oberhänsli, R., Bousquet, R., Engi, M., Goffé, B., Gosso, G., Handy, M. R., ... & Rossi, P. L. (2004). Metamorphic Structure of the Alps. *CCGM (Commission of the Geological Maps of the World), Paris.*

Philippot, P. (1990). Opposite vergence of nappes and crustal extension in the French-Italian Western Alps. *Tectonics*, *9*(5), 1143-1164.

Philippot, P., & Kienast, J. R. (1989). Chemical-microstructural changes in eclogite-facies shear zones (Monviso, Western Alps, north Italy) as indicators of strain history and the mechanism and scale of mass transfer. *Lithos*, *23*(3), 179-200.

Platt, J. P. (1986). Dynamics of orogenic wedges and the uplift of high-pressure metamorphic rocks. *Geological society of America bulletin*, *97*(9), 1037-1053.

Plunder, A., Agard, P., Dubacq, B., Chopin, C., & Bellanger, M. (2012). How continuous and precise is the record of P–T paths? Insights from combined thermobarometry and thermodynamic modelling into subduction dynamics (Schistes Lustrés, W. Alps). *Journal of Metamorphic Geology*, *30*(3), 323-346.

Polino, R. (1990). Tectonic erosion at the Adria margin and accretionary processes for the Cretaceous orogeny of the Alps. *Mémoire de la Societe géologique de France*, *156*, 345-367.

Pognante, U. (1985). Coronitic reactions and ductile shear zones in eclogitised ophiolite metagabbro, Western Alps, North Italy. *Chemical Geology*, *50*(1-3), 99-109.

Pognante, U., & Sandrone, R. (1989). Eclogites in the northern Dora-Maira nappe (western Alps, Italy). *Mineralogy and Petrology*, 40(1), 57-71.

881 Radulescu, I. G., Rubatto, D., Gregory, C., & Compagnoni, R. (2009). The age of HP metamorphism
882 in the Gran Paradiso Massif, Western Alps: a petrological and geochronological study of
883 “silvery micaschists”. *Lithos*, *110*(1-4), 95-108.
884
885 Reddy, S. M., Wheeler, J., & Cliff, R. A. (1999). The geometry and timing of orogenic extension: an
886 example from the Western Italian Alps. *Journal of Metamorphic Geology*, *17*, 573-590.
887
888 Ring, U., & Glodny, J. (2010). No need for lithospheric extension for exhuming (U) HP rocks by
889 normal faulting. *Journal of the Geological Society*, 167(2), 225-228.
890
891 Rolland, Y., Lardeaux, J. M., Guillot, S., & Nicollet, C. (2000). Extension syn-convergence,
892 poinçonnement vertical et unités métamorphiques contrastées en bordure Ouest du Grand
893 Paradis (Alpes Franco-Italiennes). *Geodinamica Acta*, 13(2-3), 133-148.
894
895 Rosenbaum, G., & Lister, G. S. (2005). The Western Alps from the Jurassic to Oligocene: spatio-
896 temporal constraints and evolutionary reconstructions. *Earth-Science Reviews*, *69*(3-4), 281-
897 306.
898
899 Rosenbaum, G., Menegon, L., Glodny, J., Vasconcelos, P., Ring, U., Massironi, M., ... & Nasipuri, P.
900 (2012). Dating deformation in the Gran Paradiso Massif (NW Italian Alps): Implications for the
901 exhumation of high-pressure rocks in a collisional belt. *Lithos*, *144*, 130-144.
902
903 Rubatto, D., & Hermann, J. (2001). Exhumation as fast as subduction?. *Geology*, *29*(1), 3-6.
904
905 Rubatto, D., & Hermann, J. (2003). Zircon formation during fluid circulation in eclogites (Monviso,
906 Western Alps): implications for Zr and Hf budget in subduction zones. *Geochimica et*
907 *Cosmochimica Acta*, *67*(12), 2173-2187.

908

909 Rubatto, D., & Angiboust, S. (2015). Oxygen isotope record of oceanic and high-pressure
910 metasomatism: a P–T–time–fluid path for the Monviso eclogites (Italy). *Contributions to*
911 *mineralogy and petrology*, *170*(5-6), 44.

912

913 Ruh, J. B., Le Pourhiet, L., Agard, P., Burov, E., & Gerya, T. (2015). Tectonic slicing of subducting
914 oceanic crust along plate interfaces: Numerical modeling. *Geochemistry, Geophysics,*
915 *Geosystems*, 16(10), 3505-3531.

916

917 Saliot, P., Dal Piaz, G. V., & Frey, M. (1980). Métamorphisme de haute pression dans les Alpes
918 franco-italo-suisses. *Géologie alpine*, *56*, 203-235.

919

920 Sandrone, R., Cadoppi, P., Sacchi, R., & Vialon, P. (1993). The Dora-Maira Massif. In Pre-Mesozoic
921 geology in the Alps (pp. 317-325). Springer, Berlin, Heidelberg.

922

923 Schmid, S. M., Fügenschuh, B., Kissling, E., & Schuster, R. (2004). Tectonic map and overall
924 architecture of the Alpine orogen. *Eclogae Geologicae Helvetiae*, 97(1), 93-117.

925

926 Schwartz, S., Guillot, S., Reynard, B., Lafay, R., Debret, B., Nicollet, C., ... & Auzende, A. L. (2013).
927 Pressure–temperature estimates of the lizardite/antigorite transition in high pressure
928 serpentinites. *Lithos*, *178*, 197-210.

929

930 Schwartz, S., Tricart, P., Lardeaux, J. M., Guillot, S., & Vidal, O. (2009). Late tectonic and
931 metamorphic evolution of the Piedmont accretionary wedge (Queyras Schistes lustrés, western
932 Alps): Evidences for tilting during Alpine collision. *Geological Society of America Bulletin*,
933 *121*(3-4), 502-518.

934

935 Schwartz, S., Lardeaux, J. M., Tricart, P., Guillot, S., & Labrin, E. (2007). Diachronous exhumation of
936 HP–LT metamorphic rocks from south-western Alps: evidence from fission-track analysis. *Terra*
937 *Nova*, *19*(2), 133-140.
938
939 Schwartz, S., Allemand, P., & Guillot, S. (2001). Numerical model of the effect of serpentinites on the
940 exhumation of eclogitic rocks: insights from the Monviso ophiolitic massif (Western Alps).
941 *Tectonophysics*, *342*(1-2), 193-206.
942
943 Schwartz, S., Lardeaux, J. M., Guillot, S., & Tricart, P. (2000). Diversité du métamorphisme
944 éclogitique dans le massif ophiolitique du Monviso (Alpes occidentales, Italie). *Geodinamica*
945 *Acta*, *13*(2-3), 169-188.
946
947 Schwartz, S. (2000). La zone piémontaise des Alpes occidentales : un paléo-complexe de
948 subduction. Arguments métamorphiques, géochronologiques et structuraux. PhD thesis,
949 Grenoble University, 287p.
950
951 Smye, A. J., Greenwood, L. V., & Holland, T. J. B. (2010). Garnet–chloritoid–kyanite assemblages:
952 eclogite facies indicators of subduction constraints in orogenic belts. *Journal of Metamorphic*
953 *Geology*, *28*(7), 753-768.
954
955 Stampfli, G. M., & Marchant, R. H. (1997). Geodynamic evolution of the Tethyan margins of the
956 Western Alps. *Deep structure of the Swiss Alps-Results from NRP 20*, 223-239.
957
958 Takeshita, H., Shimoya, H., & Itaya, T. (1994). White mica K-Ar ages of blueschist-facies rocks from
959 the Piemonte ‘calc-schists’ of the western Italian Alps. *Island Arc*, 3(3), 151-162.
960

961 Tilton, G. R., Schreyer, W., & Schertl, H. P. (1991). Pb– Sr– Nd isotopic behavior of deeply subducted
962 crustal rocks from the Dora Maira Massif, Western Alps, Italy-II: what is the age of the
963 ultrahigh-pressure metamorphism?. *Contributions to Mineralogy and Petrology*, *108*(1-2), 22-
964 33.
965
966 Tricart, P. (1984). From passive margin to continental collision; a tectonic scenario for the Western
967 Alps. *American Journal of Science*, *284*(2), 97-120.
968
969 Tricart, P., Schwartz, S., Sue, C., & Lardeaux, J. M. (2004). Evidence of synextension tilting and
970 doming during final exhumation from analysis of multistage faults (Queyras Schistes lustrés,
971 Western Alps). *Journal of Structural Geology*, *26*(9), 1633-1645.
972
973 Tricart, P., & Schwartz, S. (2006). A north-south section across the Queyras Schistes lustrés
974 (Piedmont zone, western Alps): Syn-collision refolding of a subduction wedge. *Eclogae*
975 *Geologicae Helvetiae*, *99*(3), 429-442.
976
977 Villa, I. M., Bucher, S., Bousquet, R., Kleinhanns, I. C., & Schmid, S. M. (2014). Dating polygenetic
978 metamorphic assemblages along a transect across the Western Alps. *Journal of Petrology*,
979 *55*(4), 803-830.
980
981 Villa, I. M., De Bièvre, P., Holden, N. E., & Renne, P. R. (2015). IUPAC-IUGS recommendation on the
982 half life of ^{87}Rb. *Geochimica et Cosmochimica Acta*, *164*, 382-385.
983
984 Wei, C.J., Powell, R. (2003). Phase relations in high-pressure metapelites in the system KFMASH
985 (K_2O–FeO–MgO–Al_2O_3–SiO_2–H_2O) with application to natural rocks. *Contributions to*
986 *Mineralogy and Petrology* 145(3), 301-315.
987

Wheeler, J. (1991). Structural evolution of a subducted continental sliver: the northern Dora Maira massif, Italian Alps. *Journal of the Geological Society*, 148(6), 1101-1113.

White, R.W., Powell, R., Clarke, G.L. (2003). Prograde metamorphic assemblage evolution during partial melting of metasedimentary rocks at low pressures: migmatites from Mt Stafford, Central Australia. *Journal of Petrology* 44(11), 1937-1960.

White, R. W., Powell, R., Holland, T. J. B., Johnson, T. E., & Green, E. C. R. (2014). New mineral activity–composition relations for thermodynamic calculations in metapelitic systems. *Journal of Metamorphic Geology*, *32*(3), 261-286.

White, R. W., Pomroy, N. E., & Powell, R. (2005). An in situ metatexite–diatexite transition in upper amphibolite facies rocks from Broken Hill, Australia. *Journal of Metamorphic Geology*, *23*(7), 579-602.

Whitney, D. L., & Evans, B. W. (2010). Abbreviations for names of rock-forming minerals. *American mineralogist*, *95*(1), 185-187.

Willner, A. P. (2005). Pressure–temperature evolution of a Late Palaeozoic paired metamorphic belt in North–Central Chile (34–35 30′ S). *Journal of Petrology*, *46*(9), 1805-1833.

Yamato, P., Agard, P., Burov, E., Le Pourhiet, L., Jolivet, L., & Tiberi, C. (2007). Burial and exhumation in a subduction wedge: Mutual constraints from thermomechanical modeling and natural P-T-t data (Schistes Lustrés, western Alps). *Journal of Geophysical Research: Solid Earth*, 112(B7).

Figure captions

Figure 1. **a**. Simplified geological map (modified after Schwartz, 2000) showing the main tectonic units forming the internal domain of the W. Alps in the Queyras region. Proximal and distal European continental margin fragments subducted under high pressure conditions correspond to the Briançonnais and Dora Maira complexes, respectively. Black squares: samples studied. MV: Monviso, Ro: Rocciavre. BS: blueschist-facies. Ecl: eclogite-facies. Note the presence of thin slivers of SL affinity (mafic ophiolites and associated HP metasediments) lining most of the intra-Dora Maira complex thrust contacts. **b**. Geological cross section (modified after Angiboust et al., 2012a) showing the main elements composing the HP ophiolitic nappes in the Monviso region. ISZ: intermediate shear zone, VSZ: Vallanta shear zone, BSZ: basal shear zone, USZ: upper shear zone. Serp: serpentinite. See Lombardo et al. (1978), Angiboust et al. (2012a) and Locatelli et al. (2018) for further details on the structural architecture.

Figure 2. **a**. Field view showing the main shear zone (Upper Shear Zone; USZ) separating the Monviso unit and the Lago Superiore unit in the Monviso massif, which has been re-activated as a detachment during exhumation. **b**. Representative view of the massive epidote-blueschist facies imprint recorded in Upper Shear zone metabasaltic lithologies. **c**. Picture of the exposure showing E-W oriented needles of blue amphibole (mostly glaucophane) in an epidote-rich groundmass. **d**. Representative field view of a Schistes Lustrés calcschist exposure showing that the main foliation has

1039 been locally subject to top-to-the-W shearing associated with the formation of C-S
1040 structures (Vallanta valley, hanging wall of the Monviso unit).
1041
1042 **Figure 3**. **a**. Scanning electron microscope view of a micafish showing three distinct
1043 white mica generations. The earliest, Si-rich generation is preserved in the core (Phg1),
1044 while the bulk of the foliation is composed of Phg2 (phengite 2). A muscovite-rich mica is
1045 also observed along phengite flakes lining the main foliation, in apparent textural
1046 equilibrium with paragonite (sample Vi1807, ISZ). **b**. X-ray map showing a
1047 representative view of phengite zoning in SL metasediments where cores of Phg1 are
1048 surrounded by Phg2 rims (in blue on the map; sample Vi1801, USZ). **c**. Composite map
1049 showing the BSE image in the background, a mask localizing the three different
1050 generations of white mica identified after X-ray mapping and the Ca-content of a garnet
1051 porphyroclast preserved in the main foliation (sample Ro1613). **d**. Triangular plot
1052 showing the different white mica generations identified for all the samples studied in this
1053 work. Ms: muscovite, Prl: pyrophyllite, Cel: celadonite.
1054
1055 **Figure 4**. P-T pseudosection showing phase relationships for an impure quartzite
1056 capping the top of the Monviso unit (Vi1701). P-T path (arrow and rectangle boxes) is
1057 from Angiboust et al. (2012a). Black dotted lines correspond to phengite silica content
1058 isopleths in atoms per formula unit. Yellow dotted lines correspond to garnet pyrope
1059 molar content. The white-dotted line delimitates the epidote-blueschist facies field
1060 (based on the peak blue-amphibole composition) after Evans (1990). Pie-chart gives the
1061 volumetric proportions of phases forming the assemblage prevailing along the Monviso
1062 USZ upon exhumation-related shearing. List of unlabeled assemblages: (*1*) Amp Lws Gt

1063 Cpx (*2*) Amp Lws Gt (*3*) Ctd Amp Lws Gt (*4*) Ctd Amp Gt Chl (*5*) Amp Lws Gt Chl Pg (*6*)
1064 Ctd Amp Lws Gt Chl (*7*) Amp Lws Gt Chl Fsp (*8*) Lws Gt Chl Fsp Pmp (*9*) Gt Chl Fsp
1065 (*10*) 2 Amp Gt Chl (*11*) 3 Amp Gt Chl (*12*) 2 Amp Gt Chl (*13*) 3 Amp Gt. Fields are
1066 colored from higher variance (darker) to lower variance (brighter).
1067
1068 **Figure 5**. Summary of Rb-Sr isochron plots for samples collected in the Monviso massif
1069 from the uppermost shear zone (Vallanta Shear Zone: VSZ) to the lowermost (BSZ:
1070 basal shear zone).
1071
1072 **Figure 6**. Summary of Rb-Sr isochron plots for samples collected near the base of the
1073 Rocciavre massif and in the underlying Silvery Micaschist unit.
1074
1075 **Figure 7**. Sketch showing the distribution of obtained ages, together with pie-charts
1076 showing the optically-estimated proportions of the three main generations of white mica
1077 identified as well as their average Silica content (in atoms per formula unit). (1,2,3): peak
1078 burial, eclogite-facies metamorphism ages from Rubatto & Hermann (2003), Duchêne et
1079 al. (1997), Monié & Philippot (1989) and Rubatto & Angiboust (2015), respectively. Also
1080 shown a P-T diagram showing the P-T path followed by the Monviso unit rocks (after
1081 Angiboust et al., 2012a) as well as the main white mica generations based on electron
1082 probe and thermobarometric data. Silv. Ms: silvery micaschists.
1083
1084 **Figure 8**. Simplified sketch depicting the tectonic evolution of the HP eclogite-facies
1085 nappes from the Monviso area during subduction and exhumation and relationships with
1086 surrounding units. References for the age constraints used in this figure are given in

text. Inset: D1*, D2* and D3* refer to the stages identified in Agard et al. (2001). RO: Rocciavre massif. LSU and MVU: Lago Superiore and Monviso units, in the Monviso massif. GS: greenschist-facies, ECL: eclogite-facies.

Table 1. Summary of studied samples, paragenetic information and associated Rb-Sr deformation age obtained in our study. White mica populations identified after microscopic observations and probe analyses. Conversion from surface to volumetric estimate was performed considering infinite 3D projection of 2D structures. Uncertainties on these values are on the order of ± 10 vol.%. References for P-T estimates: (1) Schwartz et al., 2013 and Agard et al., 2001; (2) Angiboust et al., 2012; (3) Groppo & Castelli (2010) and Angiboust et al. (2012a); (4) Angiboust, 2011; (5) Gasco et al., 2011; Radulescu et al., 2009. Note that for Ro1616 muscovite-rich cores were observed rimmed by Phg 1 and Phg 2.

Table 2. Representative white mica analyses from the set of studied and dated samples from the Monviso and Rocciavre massifs. bdl: below detection limits.

Appendix A. Supplementary petrographic information on studied Monviso and Rocciavre samples.

Appendix B. Full analytical Rb-Sr dataset for the samples selected for geochronological investigation.

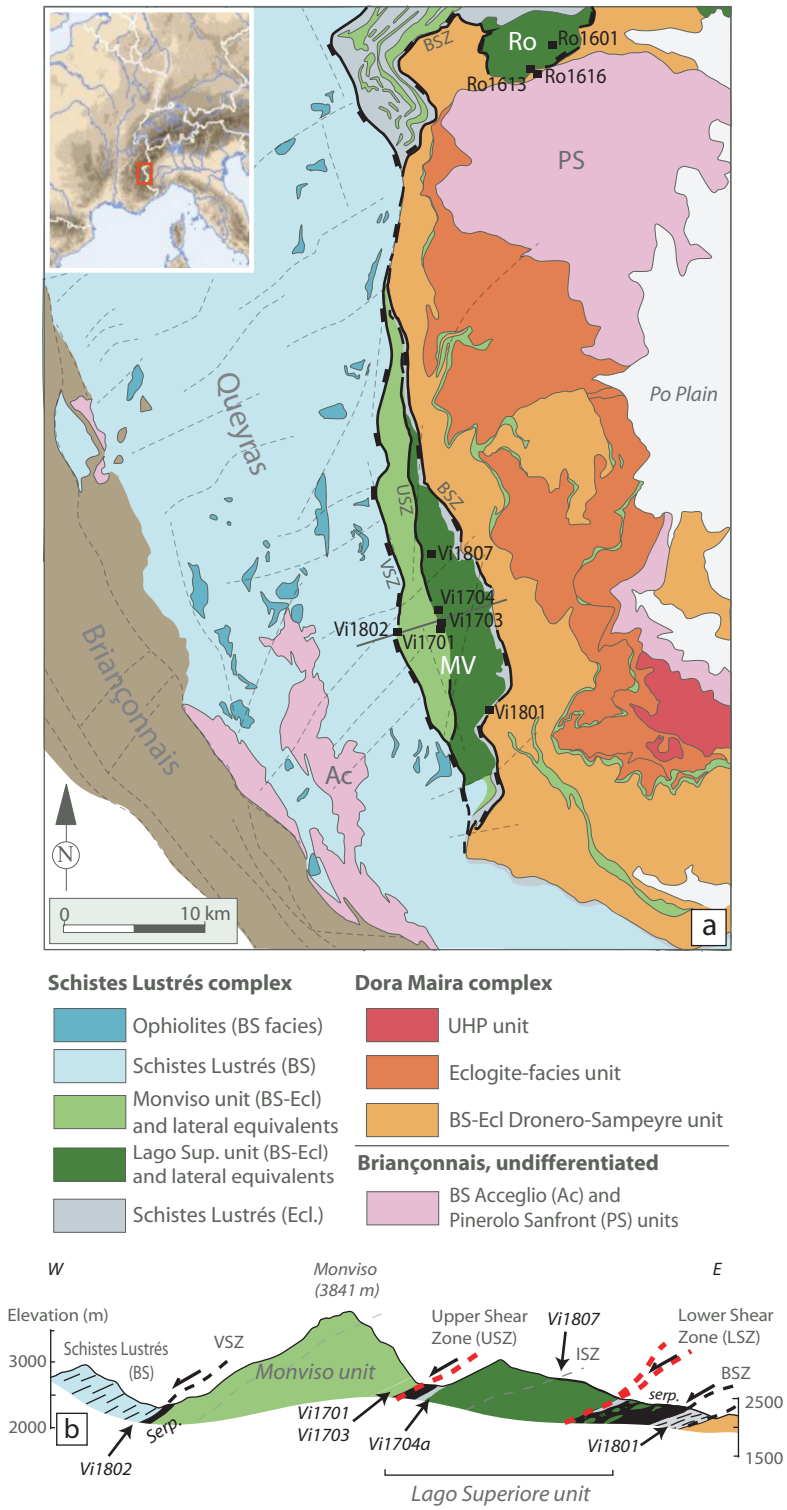
Ro
Ro1601
Ro1616
Ro1613
BSZ
PS
Po Plain
Queyras
USZ
BSZ
VSZ
Vi1807
Vi1704
Vi1703
Vi1802
Vi1701
MV
Vi1801
Briançonnais
Ac
N
0
10 km
a
Schistes Lustrés complex
Ophiolites (BS facies)
Schistes Lustrés (BS)
Monviso unit (BS-Ecl) and lateral equivalents
Lago Sup. unit (BS-Ecl) and lateral equivalents
Schistes Lustrés (Ecl.)
Dora Maira complex
UHP unit
Eclogite-facies unit
BS-Ecl Dronero-Sampeyre unit
Briançonnais, undifferentiated
BS Acceglio (Ac) and Pinerolo Sanfront (PS) units
W
E
Monviso (3841 m)
Elevation (m)
3000
2000
Schistes Lustrés (BS)
VSZ
Monviso unit
Upper Shear Zone (USZ)
Vi1807
ISZ
Lower Shear Zone (LSZ)
BSZ
serp.
2500
1500
b
Vi1701
Vi1703
Vi1704a
Vi1801
Vi1802
Lago Superiore unit

Figure 1

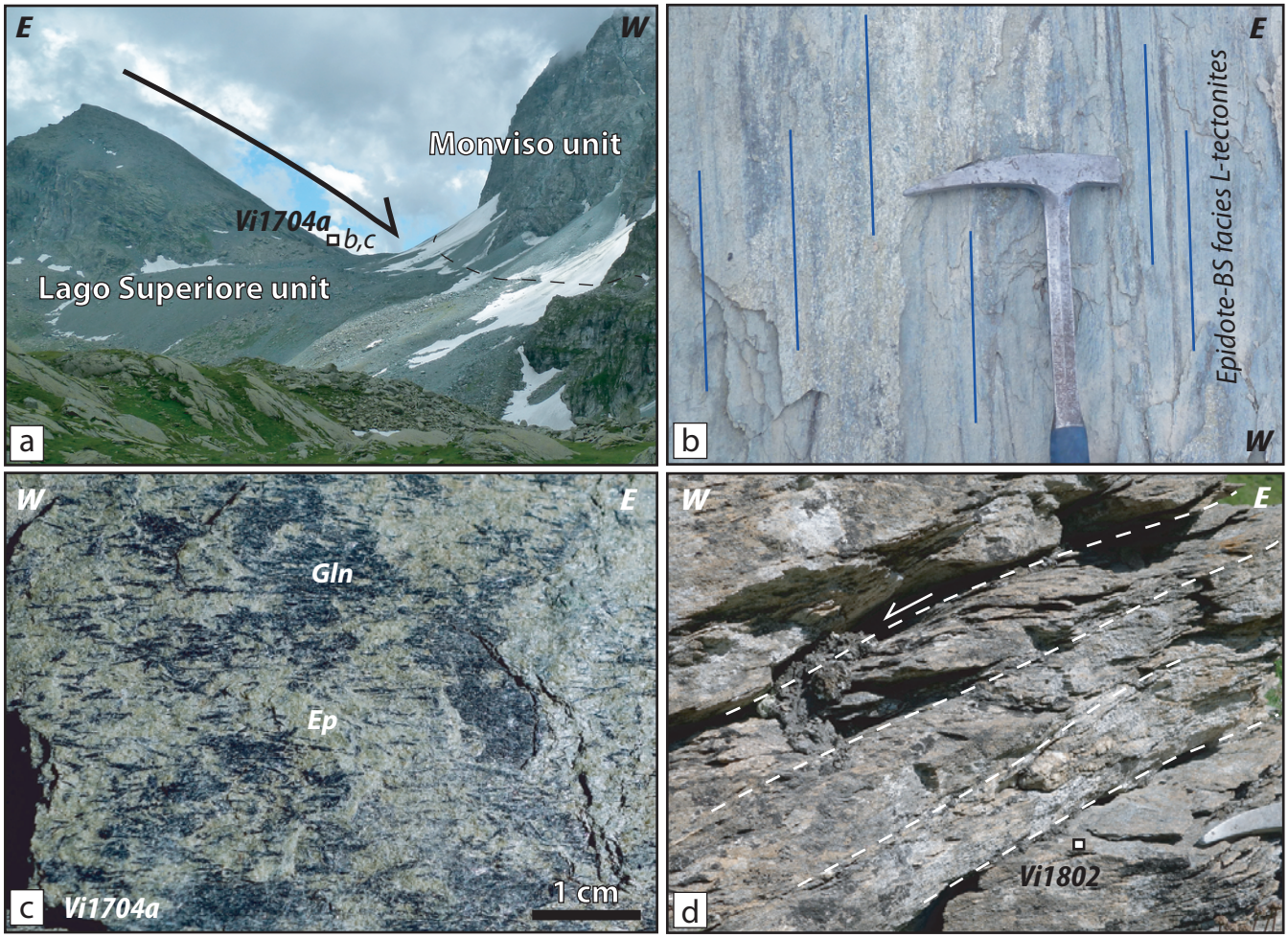
E
W
Monviso unit
Vi1704a
b,c
Lago Superiore unit
a
E
Epidote-BS facies L-tectonites
W
b
W
E
Gln
Ep
c
Vi1704a
1 cm
W
E
Vi1802
d

Figure 2

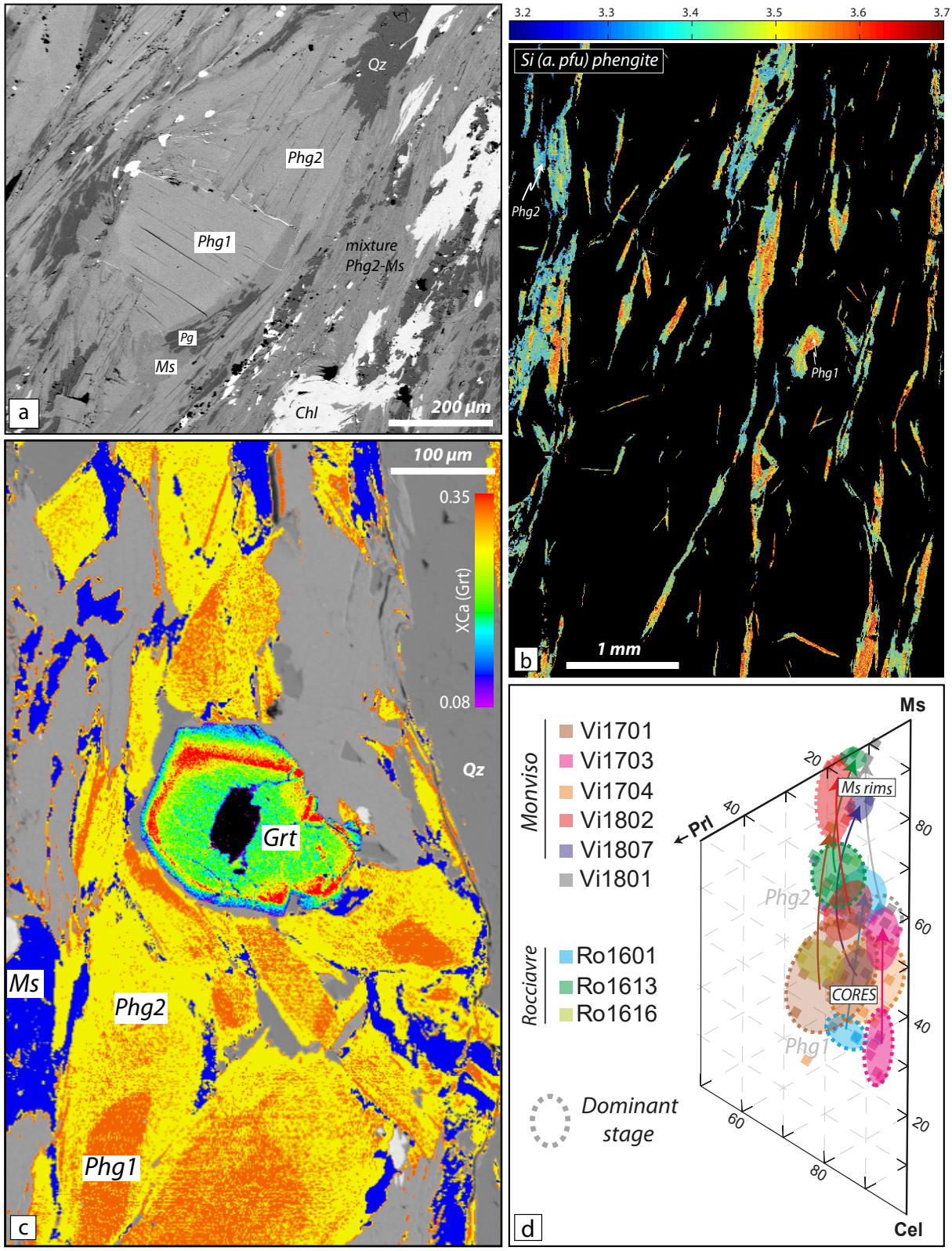
a
Qz
Phg2
Phg1
mixture
Phg2-Ms
Pg
Ms
Chl
200 µm
b
3.2
3.3
3.4
3.5
3.6
3.7
Si (a. pfu) phengite
Phg2
Phg1
1 mm
c
100 µm
0.35
XCa (Grt)
0.08
Qz
Grt
Ms
Phg2
Phg1
d
Monviso
Vi1701
Vi1703
Vi1704
Vi1802
Vi1807
Vi1801
Rocciavre
Ro1601
Ro1613
Ro1616
Dominant
stage
Ms
Prl
Cel
Ms rims
Phg2
CORES
Phg1
20
40
60
80

Figure 3

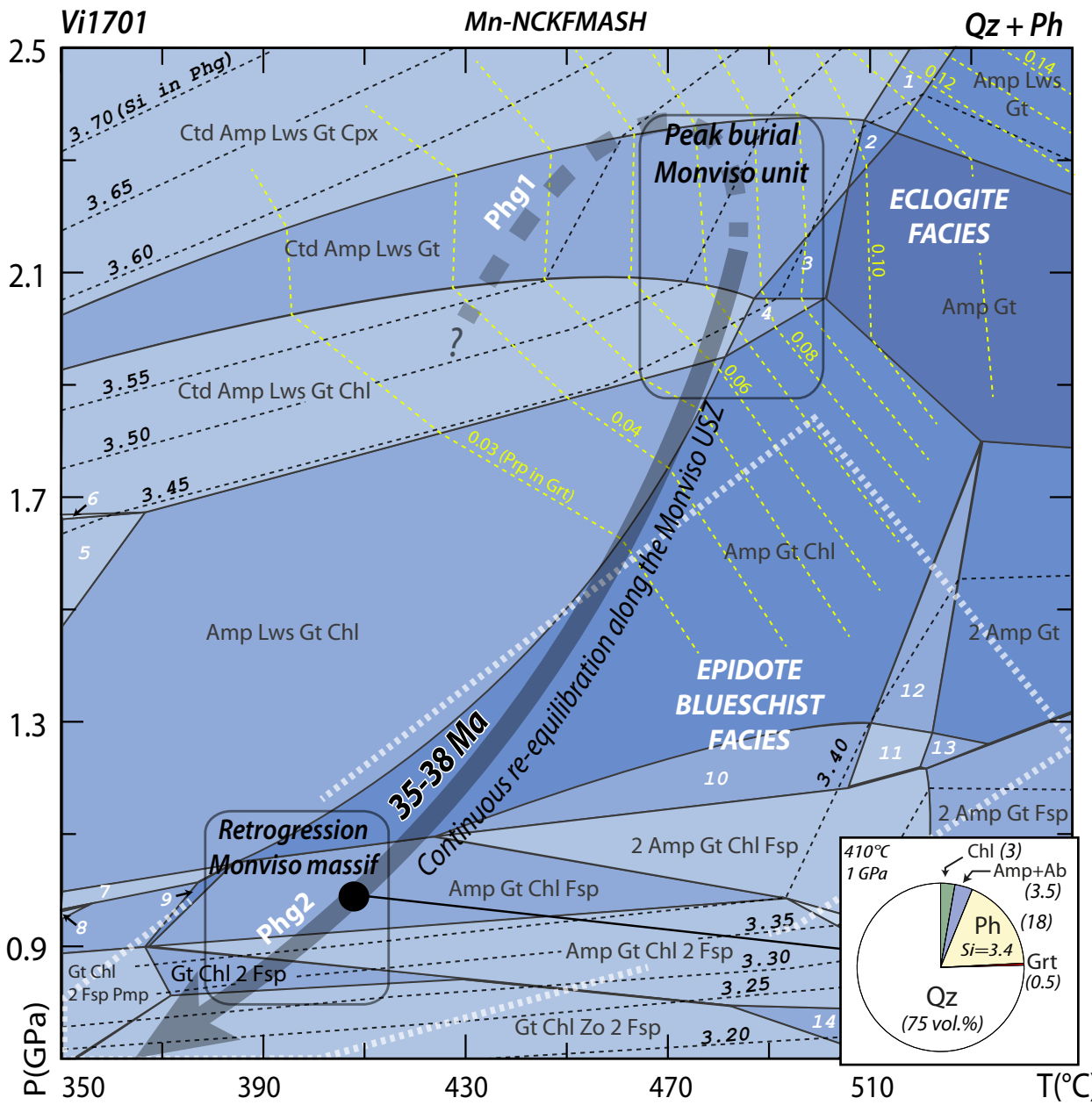
Vi1701
Mn-NCKFMASH
Qz + Ph
2.5
2.1
1.7
1.3
0.9
P(GPa)
350
390
430
470
510
T(°C)
3.70 (Si in Phg)
3.65
3.60
3.55
3.50
3.45
Ctd Amp Lws Gt Cpx
Ctd Amp Lws Gt
Ctd Amp Lws Gt Chl
Amp Lws Gt Chl
Peak burial
Monviso unit
Phg1
?
ECLOGITE
FACIES
Amp Lws
Gt
Amp Gt
0.14
0.12
0.10
0.08
0.06
0.04
0.03 (Prp in Grt)
Amp Gt Chl
2 Amp Gt
EPIDOTE
BLUESCHIST
FACIES
35-38 Ma
Continuous re-equilibration along the Monviso USZ
3.40
2 Amp Gt Fsp
2 Amp Gt Chl Fsp
Retrogression
Monviso massif
Phg2
Amp Gt Chl Fsp
3.35
3.30
3.25
3.20
Amp Gt Chl 2 Fsp
Gt Chl
2 Fsp Pmp
Gt Chl 2 Fsp
Gt Chl Zo 2 Fsp
410°C
1 GPa
Chl (3)
Amp+Ab
(3.5)
Ph
(18)
Si=3.4
Grt
(0.5)
Qz
(75 vol.%)

Figure 4

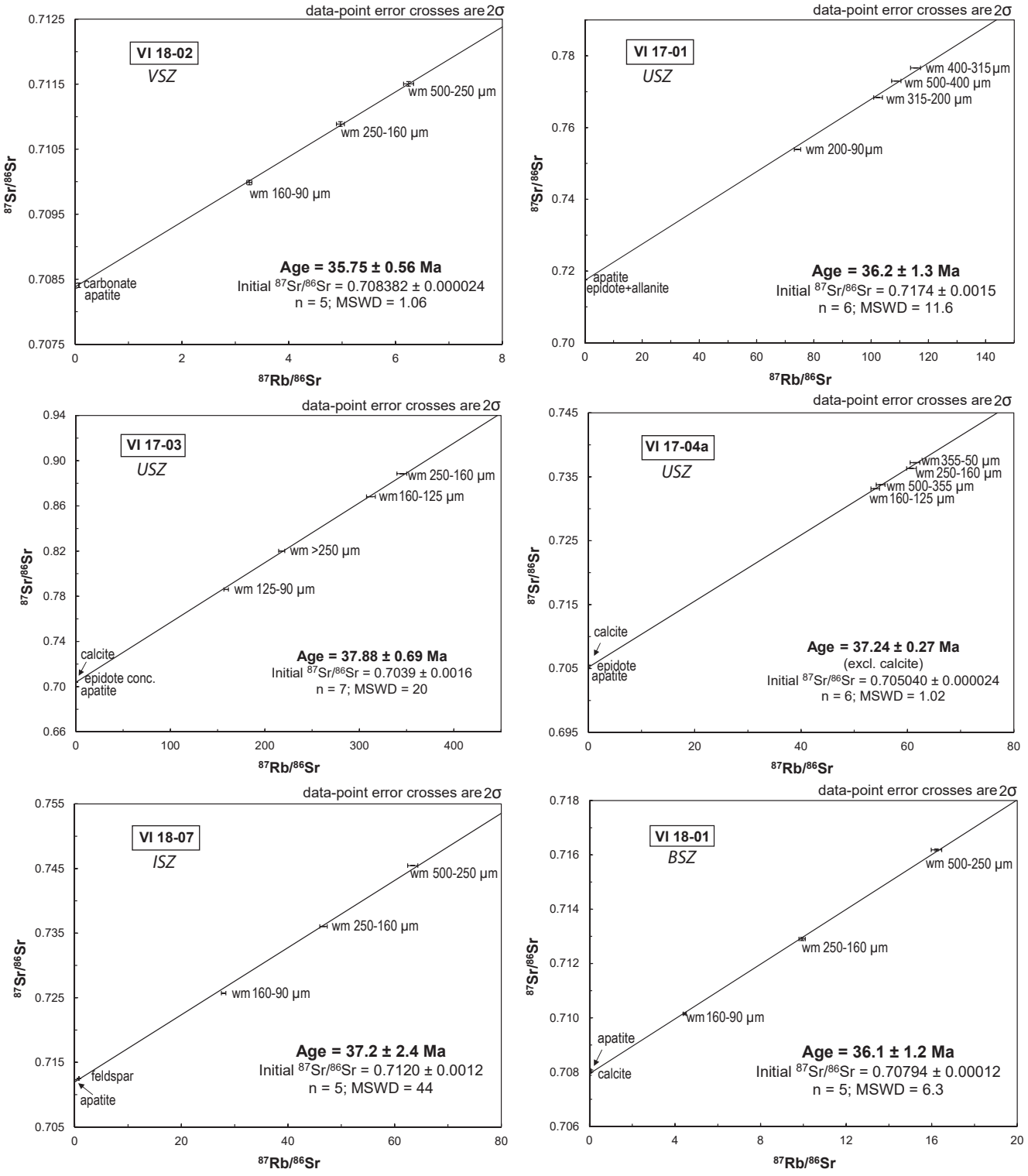
data-point error crosses are 2σ
VI 18-02
VSZ
wm 500-250 µm
wm 250-160 µm
wm 160-90 µm
carbonate apatite
Age = 35.75 ± 0.56 Ma
Initial 87Sr/86Sr = 0.708382 ± 0.000024
n = 5; MSWD = 1.06
87Sr/86Sr
87Rb/86Sr
VI 17-01
USZ
wm 400-315 µm
wm 500-400 µm
wm 315-200 µm
wm 200-90 µm
apatite epidote+allanite
Age = 36.2 ± 1.3 Ma
Initial 87Sr/86Sr = 0.7174 ± 0.0015
n = 6; MSWD = 11.6
VI 17-03
USZ
wm 250-160 µm
wm 160-125 µm
wm >250 µm
wm 125-90 µm
calcite
epidote conc.
apatite
Age = 37.88 ± 0.69 Ma
Initial 87Sr/86Sr = 0.7039 ± 0.0016
n = 7; MSWD = 20
VI 17-04a
USZ
wm 355-50 µm
wm 250-160 µm
wm 500-355 µm
wm 160-125 µm
calcite
epidote
apatite
Age = 37.24 ± 0.27 Ma
(excl. calcite)
Initial 87Sr/86Sr = 0.705040 ± 0.000024
n = 6; MSWD = 1.02
VI 18-07
ISZ
wm 500-250 µm
wm 250-160 µm
wm 160-90 µm
feldspar
apatite
Age = 37.2 ± 2.4 Ma
Initial 87Sr/86Sr = 0.7120 ± 0.0012
n = 5; MSWD = 44
VI 18-01
BSZ
wm 500-250 µm
wm 250-160 µm
wm 160-90 µm
apatite
calcite
Age = 36.1 ± 1.2 Ma
Initial 87Sr/86Sr = 0.70794 ± 0.00012
n = 5; MSWD = 6.3

Figure 5

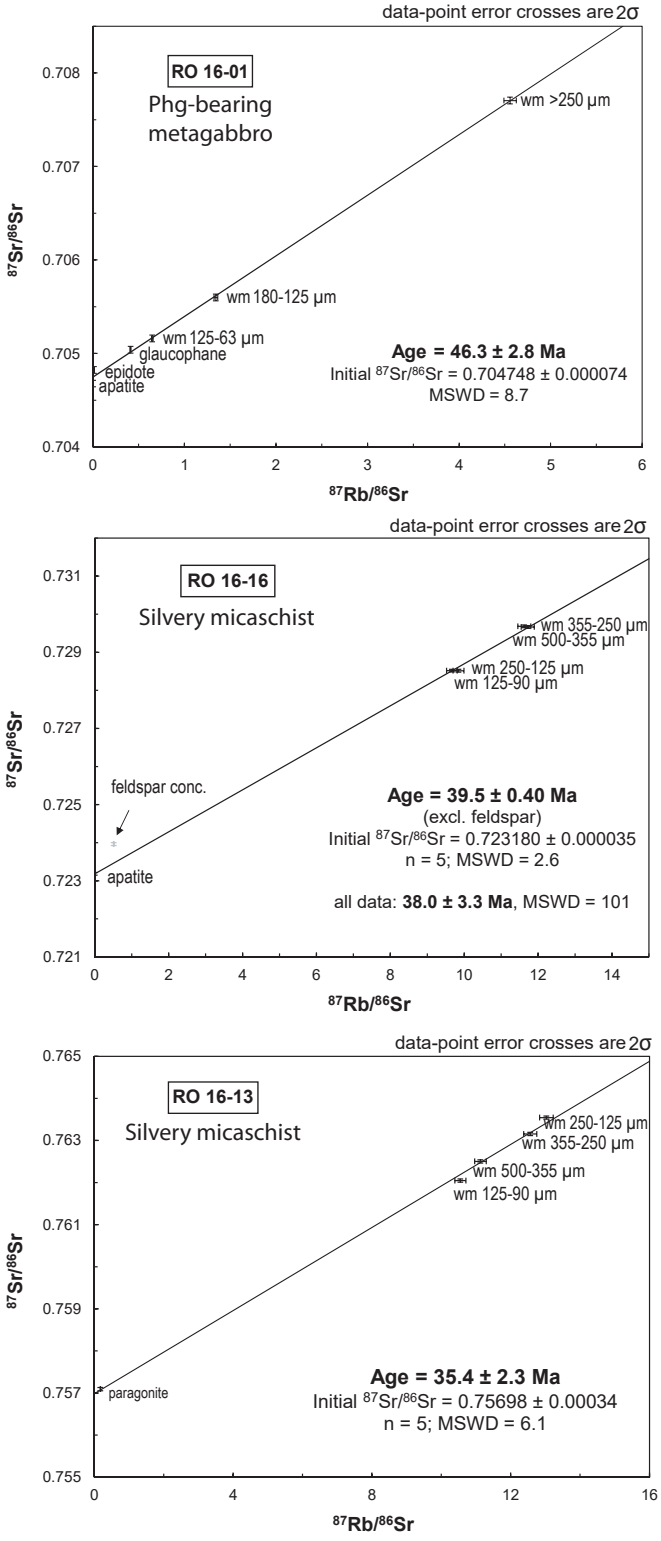
data-point error crosses are 2σ
RO 16-01
Phg-bearing metagabbro
wm >250 µm
wm 180-125 µm
wm 125-63 µm
glaucophane
epidote
apatite
Age = 46.3 ± 2.8 Ma
Initial 87Sr/86Sr = 0.704748 ± 0.000074
MSWD = 8.7
87Sr/86Sr
87Rb/86Sr
data-point error crosses are 2σ
RO 16-16
Silvery micaschist
wm 355-250 µm
wm 500-355 µm
wm 250-125 µm
wm 125-90 µm
feldspar conc.
apatite
Age = 39.5 ± 0.40 Ma
(excl. feldspar)
Initial 87Sr/86Sr = 0.723180 ± 0.000035
n = 5; MSWD = 2.6
all data: 38.0 ± 3.3 Ma, MSWD = 101
87Sr/86Sr
87Rb/86Sr
data-point error crosses are 2σ
RO 16-13
Silvery micaschist
wm 250-125 µm
wm 355-250 µm
wm 500-355 µm
wm 125-90 µm
paragonite
Age = 35.4 ± 2.3 Ma
Initial 87Sr/86Sr = 0.75698 ± 0.00034
n = 5; MSWD = 6.1
87Sr/86Sr
87Rb/86Sr

Figure 6

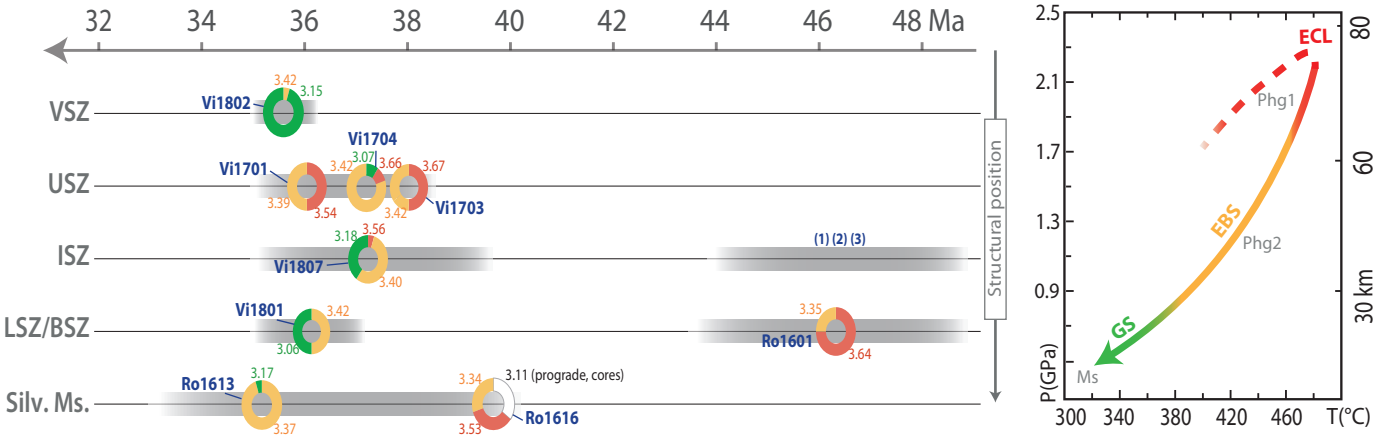
32
34
36
38
40
42
44
46
48 Ma
VSZ
USZ
ISZ
LSZ/BSZ
Silv. Ms.
Vi1802
3.42
3.15
Vi1704
3.07
Vi1701
3.42
3.66
3.67
3.39
3.54
3.42
Vi1703
3.18
3.56
Vi1807
3.40
(1) (2) (3)
Vi1801
3.42
3.06
3.35
Ro1601
3.64
Ro1613
3.17
3.37
3.34
3.11 (prograde, cores)
3.53
Ro1616
Structural position
2.5
2.1
1.7
1.3
0.9
P(GPa)
ECL
Phg1
EBS
Phg2
GS
Ms
300
340
380
420
460
T(°C)
80
60
30 km

Figure 7

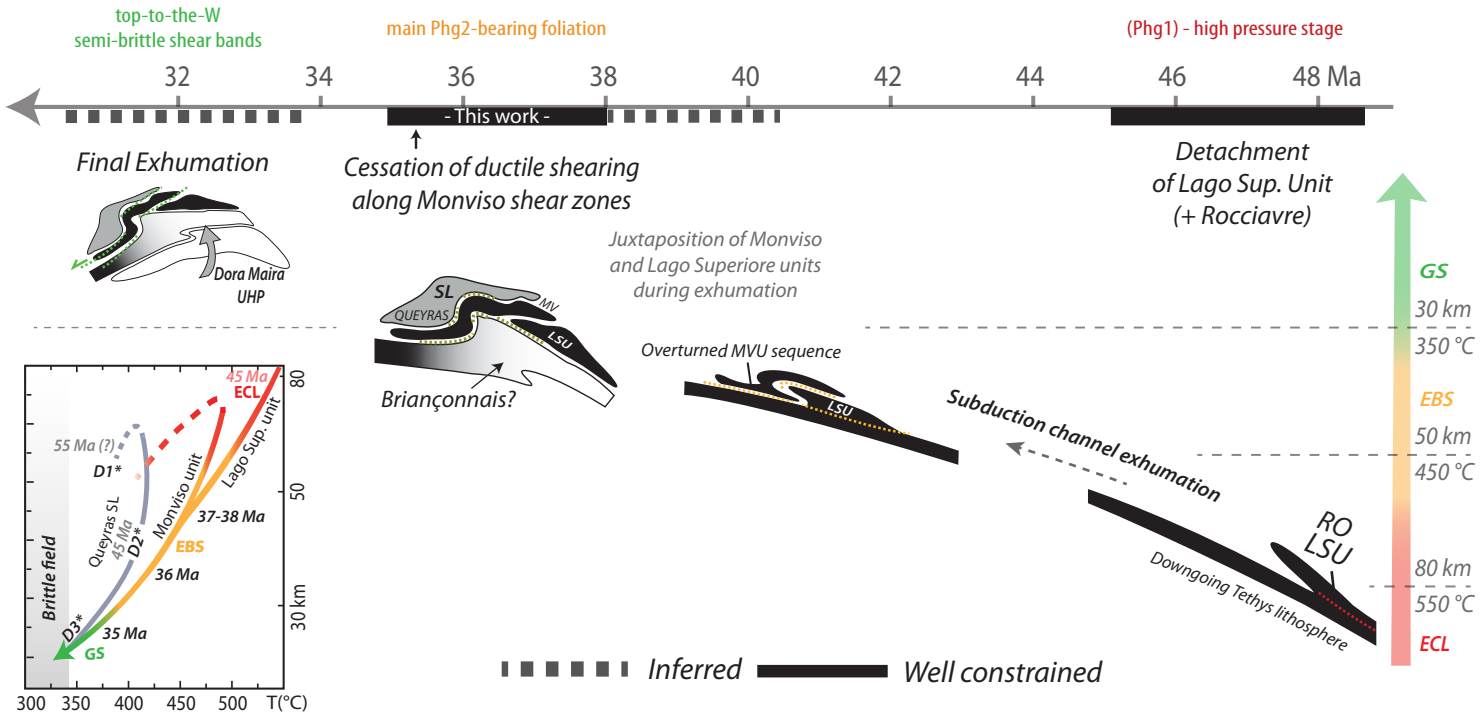
top-to-the-W
semi-brittle shear bands
main Phg2-bearing foliation
(Phg1) - high pressure stage
32
34
36
38
40
42
44
46
48 Ma
- This work -
Final Exhumation
Dora Maira
UHP
Cessation of ductile shearing
along Monviso shear zones
Detachment
of Lago Sup. Unit
(+ Rocciavre)
Juxtaposition of Monviso
and Lago Superiore units
during exhumation
SL
QUEYRAS
MV
LSU
Briançonnais?
Overturned MVU sequence
LSU
Subduction channel exhumation
RO
LSU
Downgoing Tethys lithosphere
GS
30 km
350 °C
EBS
50 km
450 °C
80 km
550 °C
ECL
45 Ma
ECL
55 Ma (?)
D1*
Monviso unit
Lago Sup. unit
Queyras SL
45 Ma
D2*
37-38 Ma
EBS
36 Ma
Brittle field
D3*
35 Ma
GS
80
50
30 km
300
350
400
450
500
T(°C)
Inferred
Well constrained

Figure 8

					White mica population (average Si content + average vol.%)		
	Sample ref.+ GPS coord.	*Unit and peak P-T*	*Retrograde paragenesis (D2)*	*Deformation age*	*Phg1*	*Phg2*	*Ms*
HP Ophiolitic domain	**Vi1802** N44° 39' 32" E7° 03' 42"	Vallanta Unit (VSZ) 450°C / 1.5 GPa (1)	Phg-Chl-Ab-Cal-Pg-Qz	35.75 ± 0.56	not observed	3.42 / 5%	3.15 / 95%
	Vi1701 N44° 39' 42" E7° 06' 19"	Monviso Unit 480°C / 2 GPa (2)	Phg-Chl-Ab-Czo-Amp-Qz	36.2 ± 1.3	3.54 / 50%	3.39 / 50%	not observed
	Vi1703 N44° 39' 42" E7° 06' 18"	Monviso Unit	Gln-Ep-Phg-Chl-Ab-Qz	37.88 ± 0.69	3.67 / 50%	3.42 / 50%	not observed
	Vi1704 N44° 40' 08" E7° 06' 29"	Lago Superiore Unit 540°C / 2.6 GPa (3)	Gln-Ep-Phg-Chl-Ab-Pg-Qz	37.24 ± 0.27	3.66 / 10%	3.42 / 80%	3.07 / 10%
	Vi1807 N44° 42' 06" E7° 05' 01"	Lago Superiore Unit	Phg-Chl-Ab-Pg-Qz	37.2 ± 2.4	3.56 / 5%	3.40 / 50%	3.18 / 45%
	Vi1801 N44° 36' 18" E7° 09' 27"	Lago Superiore Unit	Phg-Chl-Ab-Cal-Qz	36.1 ± 1.2	not observed	3.42 / 50%	3.06 / 50%
	Ro1601 N45° 01' 21" E7° 10' 24"	Rocciavre metagabbros 540°C / 2.5 GPa (?) (4)	Omp-NaAmp-Phg-Czo	46.3 ± 2.8	3.64 / 75%	3.35 / 25%	not observed
HP Cont. Margin	**Ro1613** N45° 01' 10" E7° 08' 47"	Silvery Micaschists 520-600°C / 2.0-2.7 GPa (5)	Phg-Ctd (?)-Pg-Qz	35.4 ± 2.3	not observed	3.37 / 95%	3.17 / 5%
	Ro1616 N45° 00' 59" E7° 08' 48"	Silvery Micaschists	Phg-Ctd (?)-Ab-Qz	39.5 ± 0.4	3.53 / 35%	3.34 / 35%	prograde (3.11) / 40%

Table 1

Sample #	*Vi1802*	*Vi1802*	*Vi1807*	*Vi1807*	*Vi1801*	*Vi1801*	*Ro1616*	*Ro1616*	*Ro1613*	*Ro1613*	*Vi1703*	*Vi1703*	*Vi1704*	*Vi1704*	*Vi1704*	*Vi1701*	*Vi1701*
Group	*Ms*	*Ms*	*Phg2*	*Phg1*	*Ms*	*Phg2*	*Ms*	*Phg2*	*Ms*	*Phg2*	*Phg2*	*Phg1*	*Ms*	*Phg2*	*Phg1*	*Phg2*	*Phg1*
Point ref.	*7*	*2*	*30*	*34*	*55-b*	*56-b*	*68*	*63*	*133*	*123*	*157*	*148*	*165*	*166*	*163*	*15*	*15*
SiO_2	47.49	48.05	49.00	54.35	45.70	50.83	45.42	51.97	47.26	50.52	49.77	55.77	46.93	50.32	53.51	48.64	53.04
TiO_2	0.02	0.02	0.07	0.13	bdl	bdl	0.16	0.08	0.13	0.21	0.08	0.15	0.02	0.09	0.15	0.22	0.09
Al_2O_3	36.52	38.97	33.60	23.66	36.54	27.27	35.90	26.93	36.13	27.69	26.44	19.67	36.41	22.87	21.76	29.85	23.75
FeO	0.62	0.51	1.55	4.13	0.66	2.38	1.37	2.01	1.70	2.77	2.96	4.15	1.67	4.68	4.24	4.66	3.37
MnO	bdl	0.01	0.01	0.02	bdl	bdl	0.04	0.04	0.01	bdl	0.04	bdl	bdl	0.09	bdl	0.06	0.05
MgO	0.70	0.34	1.27	3.72	1.54	3.96	0.64	3.85	0.66	2.75	3.48	5.72	0.53	4.26	4.84	1.66	4.27
CaO	bdl	0.06	bdl	bdl	bdl	bdl	bdl	0.09	0.01	0.08	bdl	0.11	0.09	bdl	bdl	0.05	bdl
Na_2O	1.06	6.74	0.62	0.00	0.99	0.31	0.87	0.19	1.11	0.23	0.37	0.01	3.33	0.06	0.04	0.47	0.20
K_2O	8.67	0.70	9.45	10.16	9.59	10.24	9.34	9.47	8.88	9.34	10.63	10.94	5.79	10.70	10.67	9.07	9.98
Total	95.08	95.41	95.58	96.19	95.01	95.00	93.72	94.63	95.88	93.59	93.76	96.51	94.77	93.07	95.21	94.68	94.75
Structural formula (based on 11 O)																	
Si	3.12	3.05	3.22	3.60	3.03	3.40	3.06	3.46	3.10	3.41	3.40	3.70	3.08	3.49	3.60	3.28	3.56
Al	2.82	2.92	2.60	1.85	2.85	2.15	2.85	2.11	2.79	2.20	2.13	1.54	2.82	1.87	1.73	2.37	1.88
Fe^{2+}	0.03	0.03	0.09	0.23	0.04	0.13	0.08	0.11	0.09	0.16	0.17	0.23	0.09	0.27	0.24	0.26	0.19
Mg	0.07	0.03	0.12	0.37	0.15	0.39	0.06	0.38	0.06	0.28	0.35	0.57	0.05	0.44	0.49	0.17	0.43
Ca	0.00	0.00	0.00	0.00	0.00	0.00	0.00	0.01	0.00	0.01	0.00	0.01	0.01	0.00	0.00	0.00	0.00
Na	0.14	0.83	0.08	0.00	0.13	0.04	0.11	0.02	0.14	0.03	0.05	0.00	0.42	0.01	0.01	0.06	0.03
K	0.73	0.06	0.79	0.86	0.81	0.87	0.80	0.80	0.74	0.80	0.92	0.93	0.49	0.95	0.92	0.78	0.85
XMg	0.67	0.53	0.59	0.62	0.19	0.53	0.45	0.77	0.41	0.64	0.67	0.71	0.36	0.61	0.67	0.39	0.69

Table 2 Representative white mica analyses